5.4
Laser-Induced Forward Transfer for the Fabrication of Devices

Matthias Nagel and Thomas Lippert

5.4.1
Introduction

In conjunction with the increasing availability of cost-efficient laser units during the recent years, laser-based micromachining techniques have been developed as an indispensable industrial instrument of ''tool-free'' high-precision manufacturing techniques for the production of miniaturized devices made of nearly every type of materials. Laser cutting and drilling, as well as surface etching, have grown meanwhile to mature standard methods in laser micromachining applications where a well-defined laser beam is used to remove material by laser ablation. As an accurately triggerable nonmechanical tool, the ablating laser beam directly allows a subtractive direct-write engraving of precise microscopic structure patterns on surfaces, such as microchannels, grooves, and well arrays, as well as for security features. Therefore, laser direct-write (LDW) techniques imply originally a controlled material ablation to create a patterned surface with spatially resolved three-dimensional structures, and gained importance as an alternative to complementary photolithographic wet-etch processes. However, with more extended setups, LDW techniques can also be utilized to deposit laterally resolved micropatterns on surfaces, which allows, in a general sense, for the laser-assisted ''printing'' of materials [1, 2].

As outlined in Figure 5.4.1, the basic setup for an additive direct-write deposition of materials is the laser-induced forward transfer (LIFT), where the laser photons are used as the triggering driving force to catapult a small volume of material from a source film toward an acceptor substrate. In contrast to the classic laser-ablation micropatterning setup where material is removed from the top surface (Figure 5.4.1a), for LIFT applications the laser interacts from the inverse side of a source film, which is typically coated onto a nonabsorbing carrier substrate. The incident laser beam propagates through the transparent carrier before the photons are absorbed by the back surface of the film. Above a specific threshold of the incoming laser energy, material is ejected from the target source and catapulted toward a receiving surface that is placed either in close proximity to or even in contact with the donor film. With adequate tuning of the applied laser energy the thrust for the forward propulsion is generated within the irradiated film volume. The absorbed laser photons cause a partial ablation of the film material, which induces a sharply triggered volume expansion coupled with a pressure jump that catapults the overlying solid material away. However, the energy conversion processes as well as the phase transitions involved in the LIFT process are complex and affected by a large number of diverse parameters. Therefore, the highly dynamic interactions between the laser and the transferred material are not easy to describe in fundamental models. Apart from laser parameters such as emission wavelength,

Nanomaterials: Processing and Characterization with Lasers, First Edition.
Edited by Subhash Chandra Singh, Haibo Zeng, Chunlei Guo, and Weiping Cai.

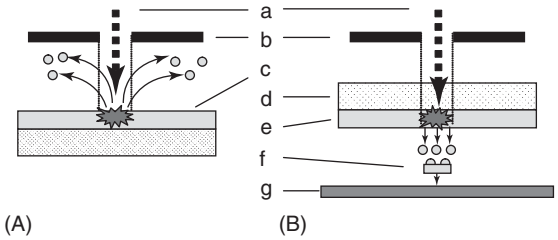

Figure 5.4.1 Conventional laser ablation (A) and laser-induced forward transfer (LIFT) setup (B), with (a) incoming laser pulse, (b) projection optics and mask, (c) surface layer of material to be ablated, (d) laser-transparent carrier substrate, (e) donor layer for transfer, (f) catapulted flyer to be deposited, and (g) receiver substrate.

pulse duration, pulse shape, focal spot size, and fluence, the properties of the transfer material system like thickness and composition, optical absorptivity, heat conductivity, thermal diffusion, viscosity, phase change behavior, and so on play an important role too. Further parameters such as the geometry of the transfer setup including the distance between the donor and receiver substrates, the properties of the carrier materials, and their surface morphology have also to be taken into consideration. For successful LIFT applications, this wide parameter space has to be specifically adapted and optimized for individual material systems to reach a smooth and controlled deposition with high resolution and conservation of integrity and functionality also of sensitive materials.

The fabrication of device structures requires the formation of complex high-resolution patterns in three dimensions with a reasonable speed. At present, commercially available, computer-controlled translation stages as well as galvanometric scanning modules enable a precise and rapid motion of either the substrates or the laser beam, and therefore the tailored direct-write deposition of small volumes of individual materials. During the past years, LIFT-based techniques have gained fundamental academic interest as complex photodynamic systems. A broad variety of device applications and demonstrators have been described in the literature, involving inorganic, organic, and macromolecular materials, and even biological systems. Since the LIFT process allows deposition of complex and multicomponent materials in one transfer step directly from a separately prepared donor substrate and without further wet-developing processes, this technique appears preferentially suitable for the fabrication of microdevices where sensitive and functional materials have to be arranged in a controlled manner without degrading their desirable properties. The following sections focus on the LIFT process for fabrication of various devices, ranging from simple metal thin-film patterns to demanding biological applications where living cells and enzymes are deposited for biosensor applications. The great versatility of the LIFT direct-write process allows the transfer of a wide range of materials and opens up new possibilities compared to conventional solvent-based deposition techniques such as screen or inkjet printing.

For the fabrication of microstructured surfaces, high-resolution photolithography techniques are far developed and well established [3], but this patterning method requires a sequence of numerous chemical processing steps, normally based on a wet-etching development of a photoresist layer irradiated by a projection mask. However, the processing conditions require chemicals and solvents that are not always compatible with sensitive materials. Therefore, further alternative nonlithographic techniques for the deposition of patterned materials on surfaces have been brought into action for the fabrication of devices, most of them based on contact or jet printing procedures.

Microcontact printing (μCP), also called *soft lithography*, uses a relief pattern on a prestructured stamp of elastomeric silicone polymers for the transfer of patterned structures of soft materials through conformal direct contact [4]. The material to be transferred has to be formulated as an appropriate ink in which the stamp is immersed before the micropattern on the receiver surface is formed by stamping [5]. This allows a precise repetitive pattern transfer for a wide range of materials that are not compatible with lithographic resist processes, for example, biomaterials and polymer precursors. Further benefits of μCP processes are comparably low fabrication and material costs, a high throughput and accuracy by automation, as well as the possibility of pattern deposition even on curved surfaces. However, μCP is a wet deposition technique, since the materials to be stamped need to be dissolved or dispersed in a suitable rheological system [6].

Screen printing (serigraphy) is a well-established method for production of graphical artwork, and has been adapted as a further wet process to deposit material patterns directly by a stencil mask technique. A fine-woven mesh stretched on a frame supports a layer of the predesigned stencil (the screen), where the stencil openings determine the 1 : 1 image that will thus be imprinted by the passing of a highly viscous ink or any other paste medium through the open areas of the ink-permeable layer onto a substrate. The ink paste is deposited and patterned in one step, but the image resolution is rather limited, with single feature sizes in the submillimeter range (down to about 100 μm). Owing to the possibility of preparing thick layers from pastelike materials, screen printing has found applications for the fabrication of electric and electronic devices on an industrial scale [7]. It is used for printing semiconducting materials and metal pastes, for example, for conducting lines on wafer-based solar photovoltaic (PV) cells, for circuit boards, and further printed electronic devices where a relatively high layer thickness, but not a high resolution, is important [8]. Nevertheless, dielectric or passivating layers for organic semiconductor devices, and even complete organic field-effect transistors (OFETs) can be screen printed, by using families of electrically functional electronic or optical inks to create active or passive devices [9]. However, the process is not very flexible since precisely structured printing masks have to be individually fabricated.

Compared to the screen printing technology, slightly higher resolutions can be achieved by inkjet printing, where small droplets of much less viscous functional inks are catapulted onto the receiver surface. Inkjet printing enables a noncontact material transfer and is a digitally data-driven direct-write deposition method that can be set up with relatively low effort (no masks or screens are needed) and also at

laboratory scale. Inkjet technology can be applied to deposit materials on substrates, but the material to be jetted must be compatible with the printhead used and must be formulated with a viscosity within a specific range [10]. Normally, the image pattern is generated by the computer-addressed two-dimensional translation of the printer head in coordination with the trigger of the droplet ejection through the nozzle orifices. Droplet deposition is well suited for low-viscosity, soluble materials like organic semiconductors, but with high-viscosity materials like organic dielectrics and dispersed particles, such as inorganic metal inks, difficulties due to clogging of the nozzles repeatedly occur. Owing to the drop-wise deposition of layers, their homogeneity is limited, and the resolution (about 50 μm) depends on the minimum droplet volume that can be deposited. The throughput is determined by the available droplet dispense rate, which typically does not exceed 25 kHz. Simultaneous usage of many nozzles as well as prestructuring of the substrate can improve the productivity and resolution, respectively. Inkjet printing is preferably used for the fabrication of organic semiconductors in organic light-emitting diodes (OLEDs) [11], but OFETs have also been completely prepared using this method [12–14]. Furthermore, biological microarrays of nucleic acids and proteins, as well as other sensing and detector devices, can be prepared by means of inkjet printing. A layer-by-layer deposition of polymer precursors allows for rapid 3D prototyping determined by digital CAD files. Three-dimensional objects and freestanding structures in the shape of each cross section can be created by successive deposition of material layers, for example, by jetting liquid photopolymers that are immediately cured after deposition by UV light. As an alternative, layers of a fine powder (plaster, corn starch, or resins) are selectively bonded by codepositing a solidifying adhesive from the inkjet nozzle head.

As a common issue, all mentioned microprinting methods require viscous inks or rheological suspension systems, and can therefore be classified as wet or solvent-based deposition procedures. At least a drying step for the solvent removal is necessary to fix the printed structure on top of the receiver surface, if not more complex annealing or even curing processes by chemical postdeposition modifications. In contrast to conventional ink-dye-based printing techniques of graphical art images, the need for a versatile deposition technology for free-forming materials [15, 16] and for multilayer devices raises a number of materials problems. Higher resolutions will be needed if organic transistor architectures are to be printed. Also, it must be possible to print bubble- and pinhole-free layers to avoid shorting of devices. Further, printing on dense rather than porous substrates requires that the ink interacts constructively with the substrate for optimum adhesion. For stacked device architectures, multiple layers must be printed such that they form discrete unmixed layers with clearly defined interfaces. Since multilayered stacks are the most favored design in device fabrication, either a strict orthogonality in the solubility of different materials or a subsequent selective cross-linking of previously solution-deposited layers is required. This solvent issue is one of the main reasons why applications of the so-called direct-write transfer methods, where solid layers are transferred from a carrier to the substrate, are of practical interest.

Laser-based methods as a preparative tool for thin-film deposition, such as *pulsed laser deposition* (PLD) [17–22] and *matrix-assisted pulsed laser evaporation* (MAPLE) [18, 23] have been developed to grow thin films of inorganic and organic materials. Both methods are based on laser ablation of a target material under vacuum conditions. On the laser interaction, inorganic materials get vaporized to form a plasma, which transports the components via the gas phase toward a receiver substrate where the redeposition process takes place. Even when such laser-based deposition methods enable the controlled growth of homogeneous thin films, they have the disadvantage that only complete layers with no lateral resolution are formed. In addition, these vapor-phase deposition processes are restricted in that they are applicable only to polymers with inherently high molecular masses, and only a few polymers have been deposited successfully by PLD with UV lasers [24–26]. This is not really surprising since UV photons will induce reactions so that such compounds tend to degrade or decompose if directly exposed to UV laser irradiation. Only polymers that depolymerize, that is, form the monomer on UV laser irradiation by a defined photochemical cleavage mechanism, may be used for this approach [27]. The deposited monomers then react on the substrate to form a new polymer film [28]. Therefore, the deposited polymer films will most probably have a different molecular weight and weight distribution than the starting material, and may also contain decomposition products. Attempts to deposit films of the biopolymer lysozyme by PLD from a solid pressed target revealed that the target crumbled up and broke into small pieces during direct mulitpulse laser exposition [29]. One possible approach to deposit thin polymer films by PLD is the application of mid-infrared (IR) radiation, which is tuned to certain absorption bands of the polymer (resonant infrared pulsed laser deposition, RIR-PLD) [30–32]. A modified approach to PLD that is more gentle is MAPLE [18, 23], which uses, in principle, the same setup as PLD, with the main difference that the target consists of a frozen solution of the polymer. The laser is then used to vaporize the solvent that is removed by the vacuum pumps while the polymer chains are propelled and deposited on the substrate. However, this approach works only for polymers that can be dissolved or dispersed in an appropriate solvent, and it should also work best when the laser is preferentially absorbed by the solvent matrix. The formation of high-quality thin films is possible, although problems with the homogeneity of the films and trapped solvents exist. Thin-film deposition of the conducting polymer PEDOT:PSS (poly(3,4-ethylenedioxythiophene)-polystyrene sulfonate) was studied with a combination of *resonant infrared laser vapor deposition* (RIR-LVD) and the MAPLE approach. The PEDOT:PSS was frozen in various matrix solutions and deposited using a tunable, mid-IR free electron laser. When adequately absorbing solvents (e.g., isopropanol and *N*-methyl pyrrolidinon) were added to the aqueous matrix, and the laser wavelength was properly adjusted to selectively excite the specific co-matrix, deposited films were smooth and exhibited electrical conductivity [33].

In the context of device fabrication, thermal evaporation processes also play an important role. Metals as well as sufficiently volatile and thermally stable organic compounds can be deposited from the gas phase within high-vacuum

chambers in the form of thin-layered two-dimensional patterns by using appropriate shadow masks. However, such vapor deposition techniques via masks suffer from the disadvantage that normally most of the evaporated material recondenses on the shadow mask area itself, and only a small part is deposited by passing the stencil apertures on the receiver surface. Therefore, a large part of the evaporated material is unproductive or even lost if not recovered. Further, small openings in the mask (as, e.g., needed for the fabrication of arrays of small pixels for display screens) tend to become overgrown by the evaporated material, and have therefore to be cleaned frequently. Printing larger areas with such delicate masks proved also to be rather difficult because of shape distortions and their weak mechanical stability. In addition, the method is essentially limited for low volatile compounds such as ionic compounds, ceramics, and polymers.

For device microfabrication, many and diverse material classes have to be integrated with a high local accuracy. In order to circumvent the above-summarized problems concerning the solvent- and vapor-based microdeposition of materials, novel approaches based on LIFT processes that enable a solvent-free (or ''dry'') direct-write deposition of solid thin films, necessary for the fabrication of devices with sensitive functional materials, have been developed. Since LIFT-based direct-write techniques are versatile with respect to the materials that can be microdeposited, such methods were developed and adapted for a variety of different device-relevant fabrication steps. For example, the deposition of micron-sized metal patterns by LIFT allows not only the direct-write of pixel masks but also the application of electrical conducting paths for electronic circuits that can simultaneously serve as metal cathodes or anodes. Mainly, inorganic compounds are used for the LIFT-based fabrication of electrochemical microcells, which are designed as small-scale energy storage and power delivery devices, such as microbatteries, microsupercapacitors, or even PV power-generating systems for remote sensors [2]. Further LIFT-fabricated microdevices include electronic on-chip circuits where semiconductor components, resistors, capacitors, and thin-film transistors (TFTs) were transferred together with metal-inks for electrical contacts. A promising extension for LIFT applications is the fabrication of organic optoelectronic devices such as color screen displays based on electroluminescent materials, or ''plastic electronic'' devices where components such as TFTs are built up with semiconducting organic and polymeric materials. Finally, a recent field of LIFT applications has been established for the fabrication of chemosensors and biosensors where biomaterials such as nucleic acids, proteins, enzymes, cells, and microorganisms have to be accurately deposited for detecting microdevice systems. Envisioned further applications include energy harvesting with thermoelectric and piezoelectric materials and radiofrequency identification (RFID) tag systems with added functionalities.

The following sections present a compilation of examples of LIFT techniques for the microdeposition of various material systems and with regard to the potential for microdevice fabrication applications.

5.4.2
LIFT Techniques for Direct-Write Applications

5.4.2.1 Traditional LIFT

As outlined in Figure 5.4.1, the donor system for basic LIFT setups consists usually of a single source material layer that has been separately precoated as a thin plane film on top of a laser-transparent carrier substrate, typically fused silica supports or polymer films, depending on the laser wavelength. A small area of the transfer material corresponding to the beam spot dimensions of a projection-mask-shaped laser is directly exposed to the incoming laser radiation, mostly applied as individual single pulses. Patterns can be generated by scanning and modulating the laser or moving the donor–acceptor stack on a computer-controlled translation stage. For an optimum laser–material interaction, the source material layer has to provide a high absorption coefficient at the laser emission wavelength, and has to be heat resistant, as well as insensitive to phase transitions and thermomechanical stress.

As far as documented in the literature, already in the early 1970s, the first demonstration of the LIFT principle was reported [34] for laser-writing image recording with common polyethylene-backed typewriter ribbons as the donor, and paper or polyester (PET) foils as the accepting substrates (Figure 5.4.2A) [35]. Compared to conventional typewriter machines or dot matrix printers, the laser-triggered scanned material transfer recording technique features an inherently noncontact, nonimpact printing system with instant viewability, and requires furthermore no process chemicals. Graphical line patterns with widths from less than 30 μm to more than 130 μm have been recorded with a 1064 nm Nd:YAG laser, depending on the focus spot size and the air gap between donor and accepting substrate, and with energy densities in the range of 1–3 J cm^{-2}. The experiments were extended further to PET-foil-supported dyes and ink materials, proving that the laser-assisted material transfer recording is not restricted to a black carbon ribbon system. Systematic studies were performed with regard to the influence of the laser

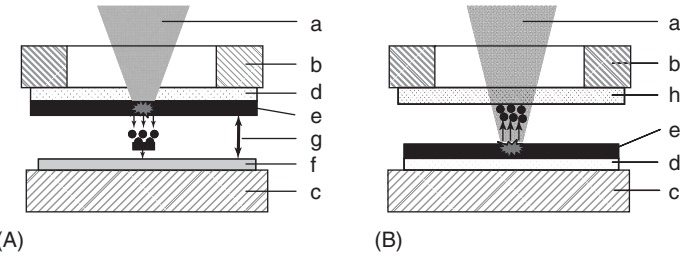

Figure 5.4.2 Two material transfer recording setups as analogously published in Ref. [35]. (A) represents the basic LIFT setup, whereas (B) shows a reversed transfer setup for a ''backscattering'' process that corresponds to a vertical pulsed laser deposition (VPLD) arrangement. The components are (a) focused and outline-shaped laser pulse, (b) front retainer, (c) rear retainer, (d) transparent polyethylene typewriter ribbon carrier film, (e) black carbon coating, (f) accepting surface of the recording medium (g) spacer gap, and (h) top receiver material transparent to laser beam.

fluence and the spacer gap distance on the quality of deposited patterns. The best resolution with smooth contours of the printed patterns was found when the donor ribbon and the accepting sheet were in direct contact.

A mechanistic model for the material transfer process involves light-to-heat conversion (LTHC) within the opaque film of dye pigments dispersed in a translucent binder matrix. Depending on the concentration of the absorbing particles, the incoming IR laser radiation propagates into the coating layer volume where it is absorbed within a certain penetration depth. The absorbed laser energy causes an ultrafast strong heating of the irradiated film volume close to the support interface, which immediately induces vapor generation by phase transitions together with shock and thermal stress waves. The vapor emission leads to an attendant buildup in pressure and induces a volume expansion together with a thermal strain. If the opaque layer is thicker than the optical penetration depth, the vaporization-built pressure will first blast a small cavity in the material layer. Finally, it breaks open the surface and delivers the momentum that catapults the spot volume toward the receiver surface. At this point, a hole in the opaque dye coating is formed, whereas the ejected material is accelerated along trajectories that depend on the pressure gradient and momentum of the expanding gas. Laser ablation itself is always accompanied by shock waves generated by the intense, nearly instantaneous thermal expansion of a point area at the surface of the illuminated material. With an air gap of about 100 μm the deposited structures showed less sharp contours accompanied by some randomly distributed particulate debris, which stems from the mechanical burst-open process of the donor film surface when the detached coating shell spot (the catapulted ''flyer''; see component (f) in Figure 5.4.1) is forward propelled. In an air gap, the propagation and even reflection of shockwaves at the receiver surface may also interfere with the ejected material, as is discussed in a later section.

Control experiments were performed with a reverse transfer setup (Figure 5.4.2B) [35] to test the differences between the two kinds of material deposition by ablation transfer. For the catapulting in the forward direction (Figure 5.4.2A) and for a given coating thickness, the transferable material was either completely removed above a certain threshold laser fluence or not at all. This observation reflects the fact that the thermal ablation process and therefore the vapor bubble formation necessary for the forward catapulting starts at the carrier–coating interface (i.e., the ''backside'' of the film). If the formed pressure is high enough, the overlying shell of the coating will fracture and be completely split off as the flyer. However, in the reverse transfer setup (Figure 5.4.2B) which works more along the classic laser ablation, small amounts of material could be removed gradually from the top surface depending on the applied laser fluence. In cases where not all of the material was removed, ablated structures in the transferable coating were observed.

5.4.2.1.1 Enhanced Donor Systems for Printing Applications

In a US patent filed in 1971 [36], a slight extension of the donor system in the printing setup is disclosed for a laser imaging application similar to that described above. The donor film coated on a transparent PET substrate comprises heat-absorbing carbon

black particles dispersed in a self-oxidizing binder consisting of nitrocellulose. The incoming IR laser heats the energy-absorbing particles and induces a blow-off or explosion of the energetic binder matrix. This causes the removal of the coating, leaving a clear area on the supporting substrate that corresponds to a positive image. If a receiver substrate is mounted as a backing in contact with the donor film, the deposited material forms an image recording. The laser power required at the focus point is sufficient only to heat the self-oxidizing nitrocellulose binder to initiate combustion. The blow-off provides the thrust to carry the carbon black particles toward the receiver sheet. Even when no details concerning the resolution and pattern accuracy are given, this example demonstrates that the laser-triggered decomposition of energetic materials can, in principle, be advantageous for the material transfer.

A further improvement of the laser-driven transfer method was disclosed in 1976 in a further patent for the preparation of planographic printing plates [37]. The formulation of the donor substrate coating contains, in addition to the above-mentioned carbon black particles and the self-oxidizing nitrocellulose binder, a cross-linkable prepolymer resin together with a thermotriggered cross-linker agent. After a laser-responsive ignition of the blow-off that causes the transfer of the prepolymer resin coating together with the cross-linking agent, the cross-linking reaction is initiated by the heat generated during the laser irradiation and the exothermic decomposition of the binder. Owing to the cross-linking reaction, the deposited polymer features are fixed after thermal curing on the receiving plate, which could directly be used for the copy printing process, whereas the donor film shows again the opposite image recording. This example demonstrates that by using appropriate material systems, in principle, laterally structured functional units such as printing plates for graphic arts can be directly fabricated by laser-assisted material transfer techniques.

5.4.2.1.2 **LIFT of Metal Patterns**

The transfer of small metal features from thin metal donor films coated on fused silica carriers by the LIFT process was first investigated by Bohandy *et al.* [38] and published in a paper in 1986 entitled ''Metal deposition from a supported metal film using an excimer laser.'' In contrast to the previous studies of graphical print applications where argon-ion and Nd:YAG lasers with emission lines in the visible and IR range, respectively, were used, metal films were irradiated with single pulses of a UV excimer laser (ArF, 193 nm emission wavelength, 15 ns pulse length), and 50 and 15 μm wide lines of copper and silver were transferred in a high-vacuum chamber from fused silica carriers precoated with metal donor films ~400 nm in thickness onto silicon receiver substrates. The experimental apparatus corresponds to the conventional LIFT setup outlined in Figure 5.4.1, which was initially placed in a vacuum chamber. With a donor–receptor distance in the range of some micrometers, deposition of metal patterns was observed above a threshold pulse energy of around 60 mJ. With increasing pulse energies, the width of the transferred line got broader, and with energies around 140 mJ more metal ''splatter'' and surrounding molten debris deposits have been observed

away from the edges of the line. As already described above, analogous control experiments have also been performed, where the metal film was irradiated through a transparent receiver substrate located in front of the film, according to the vertical pulsed laser deposition (VPLD) in Figure 5.4.2B. The metal deposits produced by that backscattering ablation experiment were found to be much worse compared to the forward transferred ones.

This study was the beginning of systematic investigations concerning the transfer mechanism and applications of the LIFT technology for the direct-write printing of conducting lines as interconnects in electronic circuit devices. One benefit of the LIFT direct-write process is the fact that the size of the written metal deposits corresponds closely to the size and shape of the laser focal spot. Mechanistic models of the laser-induced forward propulsion of metal features involve heating, melting, and vaporization of the metal film by the laser. The LIFT mechanism is triggered by the absorption of the incident laser photons at the carrier–metal interface. Depending on the surface properties and the optical constants (e.g., reflectivity R and absorption coefficient α) of the metal layer, a part of the incoming laser pulse will be reflected or even scattered, whereas the absorbed laser energy induces an ultrafast heating of the irradiated area. Owing to the high absorption coefficient α of metals, the typical penetration depths of UV photons in metal layers are typically below 20 nm, that is, the pulse energy is deposited in a very thin volume of the metal film where it gets converted into heat and leads to melting and local vaporization. Depending on the pulse length and the individual thermal parameters of both the metal layer and the underlying substrate, such as thermal conductivity, specific heat, and density, a rapid propagating phase change takes place within the film. Above a certain energy threshold, the pressure of the metal vapor that is trapped between the source film and its carrier support is high enough for a rupture of the film accompanied by the vapor-driven propulsion and lift-off of the remaining film shell [39]. For these reasons, each metal shows individual LTHC properties, depending on the combination of its inherent material properties with respect to the specific interaction with the laser and its parameters, such as the emission wavelength, fluence, pulse duration, and shape. Owing to the high thermal conductivity of metals, thermal diffusion has a strong influence on the ablation behavior, since the local heating gradient is relatively small compared to materials with a lower thermal conductivity (as, e.g., the carrier substrate). Typically, for metals and pulse lengths in the nanosecond regime the thermal diffusion length is roughly on the order of two times the optical penetration depths. For pico- and, particularly, femtosecond pulsed lasers, thermal diffusion becomes less important, and the same incident laser energy stays with ultrashort pulses significantly more localized (i.e., ''more concentrated'') in the irradiated focal point. Therefore, pulse length and beam homogeneity also play an essential role in the thermal ablation process, since the morphology and cleanliness of the resulting features and deposits is crucially influenced by the combination of all these parameters, which finally define the processing window for a successful LIFT deposition. A further problem that can be observed with the LIFT deposition of metals concerns the wettability of

the receiver surface because of the surface tension of molten metals, which often shows blurred and splashed droplet structures.

In Chapter 5.2, Sakata and Wakaki presented a compilation on general LIFT studies of various metals. In the context of device fabrication, metal deposition by LDW methods can be useful for creating conductive connections and contacts in electronic circuits by ''laser placing.'' Also, a repair of burned or interrupted interconnecting lines can be envisioned. However, as already mentioned above, the pattern quality and homogeneity of metal patterns deposited by LIFT is often unsatisfactory because of the distinct splattering and spallation behavior of transferred metal features that often appear substantially blurred by precipitation of small droplets along the rough microfeature boundaries. Recently, it was reported that for the LIFT deposition of zinc with subpicosecond pulses of a 248 nm excimer laser over a transfer gap of 100 μm the obtained structures were found to be much sharper and less blurred when the transfer was carried out in a moderate vacuum [40]. Obviously, the ultrashort pulsed UV LIFT provides a highly forward-directed material plume with only a small angular divergence in vacuum, so that only small amounts of metal is deposited outside the main track of deposited material. Nevertheless, scanning electron microscopic (SEM) images reveal at a higher magnification that the line structures are composed of many individual submicronsized droplet fragments and features, indicating that the metal film is not transferred as an intact unit.

At IBM Laboratories *laser-induced chemical vapor deposition* (LCVD) of high-purity metal films has been applied to a wide variety of microelectronics and device applications. The ability to deposit conducting materials has enabled specific applications for the laser-induced repair of ''open'' circuit defects, laser-induced deposition of interconnects for customization of circuits and the laser-based repair of high-resolution photolithographic projection masks [41]. Such masks consist of a precisely patterned thin metal layer usually coated on fused silica carriers. For the repair of clear and opaque defects in the metal mask layer material addition is needed. Besides focused ion beam (FIB) metal deposition processes, laser-induced deposition staining has been used [42]. Controlled quality thin metallic films were deposited on the defect sites by locally defined UV laser-induced decomposition of volatile tungsten, gold, molybdenum, and chromium coordination complexes as metal precursors. The optical transmission and phase-shifting properties of the deposits can be matched well to the films commonly used in phase shifting masks. But the LCVD thin-film direct-write technique is limited by the slow deposition rate, narrow choice of materials, and process complexity, including the need for operating in vacuum. For the repair of further pattern defects and trimming of microsturctures, locally resolved material removal has been performed with femtosecond laser ablation and FIB bombardment techniques.

A recent study on the creation of conductive lines by LIFT was carried out using 110 fs pulses of an 800 nm laser focused through microscopy objectives [43]. From gold donor films with a metal layer thickness between 40 and 80 nm, conductive lines with a width of 15–30 μm were written between contact electrodes. The same deposition was used to demonstrate the repair of a damaged Pt microfluidic heater

element with a small Au metal pad. Owing to the rather nanoparticulate appearance of the deposited metal, 15–40 subsequent overwrites were necessary to create lines with a peak line high of 0.6–3 μm, which showed a resistance between 100 and 400 Ω for a 1 mm long line. This is rather a high value since the porous nature of the deposited metal greatly increases the resistivity of the lines. The conductivity could be improved by a factor of 2 by gentle electrical heating by which many microdroplets are fused together, reducing conductivity bottlenecks. Thus, lines with conductivities in the range of 10^{-6} Ω m, approximately 100 times the value for bulk gold, can be produced. In an earlier study, LIFT deposition of conducting Au lines transferred with nanosecond pulses of an excimer laser from a 1.6 μm thick Au donor over a 25 μm gap resulted in 40 μm wide lines with a height of about 10 μm after 100 laser pulses with multiple stepwise overwrites [44]. While LCVD-deposited Au from metal complex precursors gave homogeneous gold lines with a resistivity about 10 times that of bulk Au, a higher resistivity was obtained from gold deposited by LIFT [41].

Since ultrafast laser pulses in the subpicosecond regime are known to have precise breakdown thresholds and minimal thermal diffusion in metals, uncontrollable melting processes are prevented, and therefore they offer advantages in precision micromachining and microdeposition applications [45]. The higher quality of the femtosecond lasers in terms of better resolution and more clearly defined morphology of the LIFT deposits has been demonstrated for the creation of diffractive optic thin-film devices in the form of binary-amplitude computer-generated hologram masks [46, 47]. With a modified 248 nm femtosecond excimer laser system, complex pixelated patterns were laser transferred pixel by pixel from a 400 nm thick chromium donor layer with a high lateral resolution of the individual square Cr deposit features of about 3 μm × 3 μm. It was also demonstrated that more than one layer of metal can be written on top of each other by creating multilevel holographic structures, comprising three layers of Cr pixels subsequently deposited. As an experimental extension, temporally shaped femtosecond laser pulses have been studied for controlling the size and morphology of LIFT-deposited micron-sized metallic structures of Au, Zn, and Cr as a function of the pulse separation time of double pulses [48]. Depending on the electron–phonon coupling in the metals, tailored pulse shaping has an influence on the ultrafast early-stage excitation processes, and this has effects on the dynamics of the ejection and deposition process.

LIFT of gold fringe patterns was achieved by projection of a laser interference pattern onto an Au-coated donor target [49]. The inherent energy distribution of the incoming interference beam has been projected as finely structured gold line patterns on the receiver substrate. This interference-based LIFT allows deposition of well-resolved structures without the need for a corresponding mask.

By using appropriate projection masks, arrays of more than one individual pixel can be deposited by one laser pulse. Simultaneous deposition of more than one small single pixel per pulse allows faster laser printing of repetitive-patterned structured and dot arrays, which, in principle, is useful for device series fabrication. A simultaneous deposition of gold multidot arrays was demonstrated by using a

target Au film that is evaporated onto a regular two-dimensional (2D) lattice of microspheres formed by self-assembly on a transparent support [50]. The Au-coated SiO_2 microspheres had a diameter of 6 μm and were irradiated with defocused single pulses of a nanosecond KrF excimer laser through the quartz carrier. Each microsphere represents a small microlens focusing the laser beam onto a small spot on the top radius where the metal film gets locally ablated. The size and index of refraction of the microspheres determine the degree of focusing and thereby the area of the illuminated gold film on the calotte of a particular sphere. Arrays of hexagonal Au dots with an average diameter of ~2.5 μm have been transferred sucessfully onto the receiver substrate. A similar setup with polystyrene microbeads as the focusing elements has been used to deposit arrays of submicron metal features [51]. A femtosecond laser emitting at 800 nm was used to deposit dotted Ti, Cr, and Au patterns. With appropriate optical parameters, deposition of submicron dot arrays could be achieved by this microbead-assisted parallel LIFT approach. However, the size of the projection mask has to fit with the laser beam diameter, and the energy distribution within the beam profile has to be taken into account. Owing to their more homogeneous beam profile, rare gas excimer lasers have therefore some advantages compared to lasers with a Gaussian-shaped energy profile.

This was recently shown with the fabrication of micron and submicron dot arrays of semiconducting β-$FeSi_2$ by LIFT with a grid-pattern projection mask [52]. Demagnification of a pinhole photomask in a UV-laser-compatible projection system down to 1 mm × 1 mm allowed the simultaneous microdeposition of highly regular dot patterns with high site control and downsized feature dimensions below 1 μm. Again, the pattern quality was found to depend strongly on the applied fluence of the 248 nm excimer laser (20 nm pulse length), and for the given system the optimum processing window had to be determined. Within the fluence range closely above the threshold fluence of transfer where the smallest regular droplets were deposited on the receiver, no corresponding apertures or holes were found in the donor layer; only bumplike curved arches have been observed on the layer surface. As an interesting contribution to the elucidation of the involved LIFT mechanism, the authors investigated the morphology of the backside interface between the source film and transparent support after irradiation. The used part of the donor film was peeled off from the support and regular concave hollows with the shape of the projected laser beam were found at the irradiated sites. The formation of these hollow gaps can be attributed to the fast phase transition processes during the laser-induced local superheating where liquefaction and gas bubble formation take place. Only a small droplet is ejected from the molten surface, whereas the remaining liquid layer freezes out again immediately and entraps the formed vapor bubble. A similar phenomenon with ''frozen'' remaining structures for laser fluences close to the ablation threshold was documented in a study on the transfer dynamics during the LIFT process of aluminum with an IR laser [53].

In order to enhance the pattern quality of conducting metal deposits and to avoid the splashing and droplet-like debris formation during the LIFT process, the effect of an additional 1 μm thick polymer coating layer on top of the 400 nm thick metal donor film was tested [54]. Unfortunately, no information has been

disclosed on the type of polymer used in this study and which laser was applied; only pulse repetition rates up to 80 kHz have been mentioned and the influence of the scan speed (obviously in the range of some tens of micrometers per second) at a fluence around 8J cm^{-2}. What happens to this overlying polymer coating during the laser-induced ejection process under these conditions has not been clearly described; however, the edge quality of the deposited patterns appears to be enhanced. It can be imagined that the polymer top coating has an influence on the metal evaporation dynamics, and modifies by that the droplet formation during the forward ejection. Also, a certain ''taping effect'' of the polymer layer to the ejected metal features can be imagined. Obviously, the polymer then gets thermally decomposed since, allegedly, by energy-dispersive X-ray spectroscopy (EDX) analyses no carbon components could be detected in the deposited metal patterns. Conducting test microelectrodes from Cr, Cu, and Al with a high of 5 μm were LIFT deposited by multiple layer-by-layer overwrites. The microstructures consist of small densely packed metal particles, showing a specific resistance of about 100 times that of the bulk metals, but also 2 times less compared to metal electrodes deposited without the auxiliary polymer top coating.

A 2 μm thick polymer coating on top of the receiver substrate was used to investigate the LIFT deposition of conducting metal interconnects into a passivation layer of electronic devices [55]. A conventional LIFT setup with silver-coated (300 nm) donor substrates and a Nd:YAG laser ($\lambda = 1064$ nm, 7 ns) was used to catapult Ag clusters into the polymeric receiver layer at an applied fluence of 1 J cm^{-2}. Usually three to five laser pulses are required to make the embedded silver particles well interconnected, forming a conducting structure in the poly(vinyl alcohol) polymer (PVA) coating. This process has been named *laser-induced implantation*. However, this technique has some differences compared to the *laser molecular implantation* (LMI) discussed in Section 5.4.3.2. The accelerated metal ejections penetrate the polymer layer surface and get embedded. Further laser pulses push the LIFT-embedded metal clusters deeper into the receiver matrix. A PVA-encapsulated TFT and a polymer light-emitting diode (LED) device have been successfully contacted via LIFT-implanted Ag interconnects. Even when the performance of the LIFT-contacted devices was somehow reduced, this approach could bear the potential for embedding electric interconnects in already encapsulated organic electronic devices during plastic substrate processing.

As an inorganic nonmetallic material, the LIFT deposition of silicon nanoparticles was recently studied with respect to potential applications in device fabrication [56]. The reported process of deposition consists of two steps each, whereby a Nd:YAG laser (1064 nm, 5–7 ns pulse width) was used: for the preparation of the donor substrates, Si nanosized particles were deposited on glass substrates by VPLD from native silicon wavers as the target material at a high-power output of the laser, according to Figure 5.4.2B. Depending on the process gas atmosphere, strong morphological variations of the deposited Si structures were observed. While in an argon atmosphere porous films of mutually agglomerated silicon nanoparticles are formed, the same procedure performed in ambient air resulted in films consisting of networks of hyperbranched nanowires of crystalline Si interconnected

by amorphous silicon oxide deposits. Both types of prefabricated donor substrates were used in the subsequent LIFT process to deposit Si-based patterns, and their morphology changes were investigated. As a test for the conservation of material functionality, fluorescence microscopy imaging was performed in order to detect luminescence emission of Si nanocrystal centers. From the analysis of the photoluminescence (PL) spectra, a core–shell structure of the deposited Si nanoparticles was derived where excitons are trapped in a confinement at the Si/SiO_2 interface.

LIFT of Metal Nanoparticle Inks LDW of conductive metallic interconnection lines is of great interest for the tailored fabrication of electronic microdevices and printed electronics. During the past years, inkjet technology of metal nanoparticles was essentially developed, including the delicate thermal postprocessing steps for the fixation and functionalization of the inkjetted structures by curing and annealing. However, for inks with high contents of nanoparticles indispensable for the creation of well-conducting lines, the inherently high viscosity of such inks makes it more difficult to be applied by small-orifice nozzles in inkjet printers because of their tendency to clog and contaminate [57]. Here, the LIFT of viscous pastes can offer a promising technical improvement. The opaque ink has a high absorption coefficient, and the metal nanoparticles provide an efficient interaction with the laser so that only a portion of an ink donor layer would be vaporized to catapult the remaining coating. While the binder matrix of the paste serves only as an auxiliary compound that has anyway to be modified or removed later by a separate curing step, a chemical alteration by the LIFT process might not be so relevant. Depending on the composition of the ink, the binder matrix can be more or less volatile and adapted to an appropriate viscosity of the paste so that the fluid dynamics of the ejected features can be finely adapted toward a proper jetting and deposition behavior. In addition, tuning of the rheologic properties of the ink paste enables the deposited single-droplet features to flow and coalesce, and form by that continuous pattern structures for conducting lines. Highly viscous nanoparticle pastes enable a defined LIFT catapulting process of elastic soft patterns, which are transferred homogenously without morphological changes by droplet formation and deposited without splashing.

Silver nanoinks containing 20–50 wt% of Ag particles with a size below 100 nm were used for corresponding LIFT direct-write printing experiments [58]. A frequency-tripled $Nd : YVO_4$ laser with an emission at 355 nm and about 30 ns pulses was used to transfer the nanoink coating from a glass support toward Si wavers or polyimid (Kapton®) foils. Postdeposition curing treatment was carried out either by thermal curing in an oven for 40 min at 250 °C or with laser baking. Continuous lines, ~20 μm in width and ~0.5 μm in height, with good particle agglomeration could be obtained by that procedure. Lines of 470 μm in length printed between two gold electrodes on Kapton exhibited good electrical conductivity with a resistivity of less than 10 times that of bulk Ag.

Conducting lines were also LIFT printed with a pulsed IR laser using a commercially available Ag/Pt-nanoparticle-based ink (QS 300 manufactured by DuPont)

[59]. This ink has been developed for industrial microelectronic screen printing applications for producing fine lines down to 75 μm with contact masks. The rheology of such screen printing inks is specifically designed to vary with the shear forces applied to the ink. In the absence of shear forces, the ink is very viscous (thixotropy) so that deposited patterns can resist distortions once they are deposited. For the preparation of donor substrates, the ink was mixed with α-terpineol as a less-volatile solvent to get a modified matrix that was used earlier for a matrix-assisted pulsed laser evaporation direct-write (MAPLE-DW) study with inorganic powders and a 355 nm UV laser [60]. A complex fluid dynamic behavior has been observed on pulsed irradiation with a neodymium-doped yttrium lithium fluoride (Nd:YLF) laser at 1047 nm emission wavelength, including a bubble protrusion, jetting, and plume regime, depending on the surface tension of the film. Only within the bubble protrusion regime could a sufficient transfer be achieved, since considerable instability of the jet was observed in the more energetic regime, and the ejected ink splattered on contact with the receiver substrate. Without the additional solvent, the ink proved to be too viscous for thin-film fabrication by spin coating or wire coating. Therefore, the donor films were thicker and did not form a jet anymore. However, line features as small as about 20 μm could be deposited, which showed conductivity after high-temperature curing of about 75% of the specified value for conventional screen printing.

A further enhancement of the transfer pattern quality was obtained by using designed silver nanoparticle (Ag NP) inks with significantly increased viscosity [61, 62]. In the LIFT process, since the ink need not pass a small nozzle channel to be jetted on the receiver, ink pastes with much higher viscosities and a higher nanoparticle content can be employed, similar to that used for screen printing. A paste of small colloidal Ag nanoparticles (size 3–7 nm) with a viscosity of ∼100 000 cP was used for printing pixel patterns and line structures with the third harmonic emission at 355 nm of a Nd : YVO_4 laser at fluences of 8–40 mJ cm^{-2}. The donor layer was coated with a 100–300 nm thick layer of the ink suspension and the transfer gap was adjusted between 10 and 50 μm. Unfortunately, no information is disclosed on the composition of the binder matrix of that Ag nanoparticle paste, so that no conclusions can be drawn about the laser–ink interaction and the energy conversion that results in well-defined pixel deposits. It may be assumed that the UV laser excites the quantum-size-effect-dependent absorption of the Ag nanoparticles, inducing an LTHC that causes the thrust for the transfer by decomposition of the thermocurable binder matrix. A thermal postdeposition curing of the transferred patterns was carried out either by *in situ* laser treatment (scanning with a 532 nm continuous wave (CW) laser) or in a convection oven at 200 °C for 30 min. Since the deposited pixels showed clearly defined edges without debris and with a homogeneous shape morphology in correspondence with the remaining ablated spots on the donor substrate, the method was called *laser decal transfer* (derived from ''decal,'' which is a plastic, cloth, paper, or ceramic substrate that has printed on it a pattern that can be moved to another surface on contact, usually with the aid of heat or water). Conducting line structures were built either by continuous deposition of individual pixels close to each other or by stacking

two layers to bridge gaps between pixels. The resistivity of such structures after thermocuring was found to be up to about two times that of bulk silver. Even freestanding, 25 μm long and 5 μm width bridging silver structures could recently be deposited over microchannels by this approach [63].

However, since such nanoinks consist of more than only one component, that is, the metal nanoparticle dispersion in the ''wet'' binder matrix one may note that the mechanism of such a transfer process differs in principle from the above-discussed basic LIFT technique where normally coatings of only one material are used for transfer. Owing to the role of the thermodegradable binder system, this application has some close analogy with the so-called MAPLE-DW process discussed in Section 5.4.3.1. A suspension of Ag NPs was also used as a laser-absorbing dynamic release layer (DRL) for the transfer of organic electronic materials, as described later in Section 5.4.3.3.5) [64].

5.4.2.1.3 LIFT of Organic Materials

Since the entire transfer material itself is directly exposed to the laser radiation in the basic LIFT process, the transfer conditions for the material to be deposited are rather harsh with respect to thermal load and photochemical impact that may cause structural alterations. As shown for metals, thermally induced phase transitions may have a strong and often detrimental influence on the quality and homogeneity of the transferred features, even when ultrashort laser pulse lengths are applied. Therefore, mostly robust and heat-tolerant compounds, such as inorganic oxides, ceramic, and dielectric materials were used for transfer studies. Nevertheless, examples can be found in the literature where organic materials were deposited successfully, but preferably by using ultrashort laser pulses in order to circumvent detrimental heat diffusion within the donor material coating. For applications where bulk properties of the transferred material are important, the decomposition of a more or less ''thin'' top layer of the sensitive material may be acceptable, but this is not the case for all applications, such as sensors, where the surface properties of the layers are decisive.

LIFT of Small Organic Molecules The LIFT deposition of the pink-colored laser dye Rhodamine 610 was investigated with the second harmonic emission of a Nd:YAG laser at 532 nm [65]. When the transfer was carried out at low fluences and in vacuum over a gap of ~15 μm, corresponding pink deposits were found on the SiO_2 receiver surface, accompanied by black debris particles. As a check of the chemical integrity of the transferred molecules, fluorescence measurements were performed. It was found that for a transfer performed in air the fluorescence intensity was only quite weak, whereas under vacuum conditions a moderate intensity could be detected. Obviously, the thermal impact in an oxidizing atmosphere is rather destructive to the chemical structure of the dye, but at low pressure and in an oxygen-free environment a transfer seems feasible. Possibly, due to the reduced pressure the thermal sublimation of dye molecules is facilitated, in analogy with other thermal deposition techniques, such as chemical vapor deposition (CVD) and also PLD, which are known to be applicable to the fabrication of thin-film

coatings of small organic molecules [66–68]. However, the fluorescence intensities after LIFT of the same dye component was significantly higher when the transfer was carried out with a modified donor substrate where the dye is coated on top of an additional intermediate thin gold metal film that absorbs the incoming laser pulse. This modified metal-film-assisted LIFT technique is discussed in Section 5.4.3.3.3.

A LIFT-fabricated organic TFT device could be fabricated by depositing patterns of the organic p-type semiconductor copper phthalocyanine (CuPc), which is known as a chemically and photochemically robust metalorganic material [69]. The UV–vis absorption spectrum of CuPc shows a band around 355 nm, giving rise to absorption depth of about 85 nm of the corresponding emission wavelength of a pulsed Nd:YAG picosecond laser. The LIFT deposition was achieved from 100 nm thick CuPc donor films on fused silica (Suprasil) at a fluence of 100 mJ cm^{-2}, resulting in laterally well-resolved square deposits. Source and drain electrodes have also been LIFT printed using a commercially available Ag NPs ink. The electrical characteristics and parameters of devices fabricated by LIFT with CuPc as active layer were not so far from devices made by conventional evaporation of CuPc and silver electrodes.

LIFT of Carbon Nanotubes In close analogy with the very first reported LIFT deposition of black carbon ink recordings, carbon nanotubes (CNTs) as one further carbon modification were transferred to form functional patterned arrays that work as field emission cathode devices [70]. A precoated 20 μm thick film of CNTs with diameters ranging from 20 to 40 nm was used as the donor layer, which was exposed to 10 ns pulses of a 1064 nm Nd:YAG laser. Arrays of 27 × 27 dots were transferred to a conductive indium–tin oxide (ITO)-coated glass substrate by using a 80 μm thick sieve-type through-hole contact mask with a grid pattern of small holes. Donor, hole mask, and receiver were held in close contact during the single-pulse laser irradiation at a fluence of about 320 J cm^{-2} and in ambient environment. After peel-off of the patterning mask a CNT dot array with sizes of the single bump features of ~10 μm was obtained. Such dot arrays with different thicknesses of the deposited dots were tested as field emission cathode devices where a light emission could be demonstrated if a DC voltage up to 1100 V was applied. Obviously, the field emission properties were not suppressed by the laser interaction of the CNTs during the transfer.

LIFT of multiwall carbon nanotubes (MWCNTs) dispersed in various water-soluble polymer host matrices was studied recently with single pulses of the frequency-quadrupled emission at 266 nm of a Nd:YAG nanosecond laser [71]. Polymer composites were prepared by dispersing two types of MWCNTs in either poly(acrylic acid) or poly(vinylpyrrolidone). Owing to the inherent hydrophobic properties of MWCNTs, chemically functionalized MWCNTs that bear carboxyl groups on their surface were used to enhance the solubility in aqueous media, and to avoid the well-known agglomeration and aggregation behavior of MWCNTs in hydrophilic solvents. About 1.5 μm thick films of the polymer/MWCNT composites were fabricated by spin coating, which show a strong and broad

UV absorption around 250 nm because of the electronic structure of the CNTs. Only LIFT composite films with the functionalized MWCNTs that are much more homogeneously dispersed in the donor target matrix gave reproducible deposits, whereas agglomerates of unmodified MWCNTs in the composite donor films resulted in an inhomogeneous local absorption distribution of the laser energy, and therefore to discontinuous LIFT deposition results. Deposited composite pixels with an MWCNT content up to 10% showed sufficient electrical conductivity. With the versatile variability of functional polymeric host materials, laser-based direct-write deposition of conducting metal-free microstructures based on designed composite materials has a broad potential for applications in organic electronics and sensing device fabrication.

LIFT of Polymer Films Since polymers are macromolecular compounds that have inherently high molecular masses they normally cannot easily be thermally evaporated or sublimed without substantial decomposition, even under ultrahigh vacuum conditions. For photochemical, photothermal, or photophysical ablation with laser photons the polymers need to have corresponding radiation-absorbing chromophore moieties incorporated in the repeating units. Most of the common commercial polymers have only a weak absorbance in the IR and visible domain. Absorption in the UV range induces electronically excited molecular states that often induce the cleavage of chemical bonds, and lead therefore to polymer photodecomposition and degradation into various small fragments. Since the first reports on polymer ablation with UV lasers in 1982 [72], laser polymer processing has become an important field for various microfabrication applications, mainly for ablative structuring and pinhole drilling. The main parameters that describe polymer ablation are the ablation rate $d(F)$, that is, a certain ablation depth d obtained with defined applied laser fluence F, and the ablation threshold fluence F_{th}, which is defined as the minimum fluence where the onset of ablation can be observed [73]. The linear absorption coefficient $\alpha_{lin}(\lambda)$ represents the wavelength-dependent spectroscopic absorption properties for a given film thickness, determined under static irradiation conditions with light intensities far below the ablation threshold. Many single-pulse ablation processes can be approximately described by the following equation:

$$d(F) = {\alpha_{eff}}^{-1} \ln(F/F_{th})$$

where α_{eff} represents the so-called effective absorption coefficient for laser ablation, which links as a wavelength-, material-, and process-dependent index factor the observed ablation rate $d(F)$ with the applied laser fluence, and depends further inherently on the pulse length. All these parameters have to be taken into account when a polymer film is catapulted and deposited according to the LIFT method. However, without further modifications, at least a part of the entire polymer layer has to be sacrificed for the generation of the pressure necessary for the LIFT process. If an appropriate amount of small molecular fragments are generated by ablative laser-induced polymer decomposition close to the carrier substrate, the overlying part of the film can be forward ejected by the pressure buildup within the ablated volume. However, the top surface of the LIFT-deposited film will be modified or even damaged since it

is the laser-exposed side of the donor target that gets partly ablated. Owing to the restricted parameter space and the sensitivity of polymeric materials, it proved rather difficult to find optimum conditions for an ablative LIFT deposition of polymer films without chemical degradation or significant deterioration of their physical properties.

The direct LIFT transfer of entire thin films of the conjugated polymer PEDOT:PSS, which is used as a conductive polymer coating in stacked electronic thin-film device architectures, was exemplarily studied with different laser wavelength and pulse durations [74]. About 300 nm thick polymer films on glass or fused silica carriers were used as donor targets and irradiated with 8 ns pulses of an 1064 nm Nd:YAG solid-state laser. Owing to a certain absorbance in the IR, the donor film could be ablated from the donor carrier, but a pixel deposition onto the receiver substrate could only be reached at higher laser fluences that cause severe traces of thermal stress and morphological surface alterations, and even damage to the flexible plastic receiver surface was observed. This indicates that only a part of the laser radiation was absorbed by the film, and the whole film volume was penetrated (and therefore heated) by the laser photons. With the second harmonic of the same laser at 532 nm, the transfer was much worse because of the much lower absorption of the film in the visible radiation domain. Only 25% of the incoming light is absorbed, and by that ablation of the film from the donor was only possible with quite high laser fluences that destroyed the film without getting acceptable deposits. PEDOT:PSS is strongly absorbing at the 248 nm emission of a UV excimer laser, and the LIFT deposition of well-defined coherent pixels can be performed at comparably low laser fluences, however, only in a very small fluence range, and with loss of the electrical properties of the conjugated polymer due to photochemically induced alterations. Trapped bubbles and pinholes in the deposited film can be seen as an indicator of the formation of small volatile fragments during laser ablation, which form a pressure pocket during irradiation of the film and diffuse into a thin polymer layer before it is forward propelled by the generated thrust. In summary, direct LIFT of thin polymer films proved difficult to obtain without substantially destructive side effects, and examples in the literature are hitherto rare.

LIFT of Biogenic Materials Subpicosecond laser pulses of a modified 248 nm KrF excimer laser were used to study the direct-write LIFT printing of microarrays of entire biomaterials, such as DNA [75] and enzymes [76]. Since thermal effects detrimental to the irradiated material can be kept much smaller with smaller laser pulses compared to conventional nanosecond laser pulse durations, destructive effects on the absorbing material are less prominent during the LIFT process. Therefore, even delicate organic materials can be taken into account for LIFT deposition. Dynamic multiphoton absorption effects may additionally contribute to enhanced absorption properties of the irradiated material, and therefore to limit the propagation depth of the incident laser pulse within the transfer material. With such a reduced penetration depth and a much more locally restricted heat load, a higher fraction of sensitive transfer materials suffers less intense effects caused

by the laser impact, enhancing the probability that delicate material systems can also be forward transferred without functional damage to their desirable properties. For microdevice fabrication, not only the quality of transferred patterns with respect to local resolution, feature morphology, and homogeneity play an essential role but also, in particular, the conservation of desired functional properties of the deposited material systems. Therefore, a check of material integrity, physical functionality, or activity after laser transfer is crucial to judge or even quantify whether a successful transfer was obtained. For biogenic materials systems, sophisticated immunochemical indicators and highly specific probe reactions were developed based, for example, on labeled antigen–antibody reactions or enzyme activity measurements that can be performed with very low concentrations and at microscale dimensions.

Horseradish peroxidiase (HRP) was used as a model enzyme for LIFT deposition [76]. In conjunction with hydrogen peroxide (H_2O_2) as the chemically active oxidizing agent, HRP efficiently catalyzes oxidation reactions. The presence and enzyme activity of HRP can be made easily visible and detectable by spectrophotometric methods when, by such oxidation reactions, a colorless compound (a leukodye) is converted into visible chromogenic product molecules that can then be physically detected. In addition, in the presence of luminol as cosubstrate the HRP-catalyzed oxidation results in a direct light emission by chemoluminescence (428 nm). With appropriate experimental conditions, this allows a quantitative and locally resolved measurement of the enzyme activity. By a corresponding staining reaction after LIFT printing of HRP micropixel patterns with subpicosecond UV pulses, it was demonstrated by confocal laser fluorescent scanning that the enzyme remained active after the LIFT process. However, in the referred paper no quantitative data are presented about the relation of enzyme activity before and post transfer.

Transferring DNA material was also demonstrated with the application of subpicosecond pulses of a UV laser [75]. Double-strand DNA molecules extracted from lambda phage particles have been used as the test material. Before coating on the donor support, the DNA strands were labeled with a fluorescent dye (Alexa 594) for detection by scanning laser confocal fluorescence microscopy after two-dimensional arrays have been LIFT printed. It could be shown that sufficient fluorescence intensity could be detected from the deposited arrays. Electrophoretic blot analysis of the DNA after an enzymatic restriction process showed a distribution pattern quite similar to the single fractions without a significant enrichment of oligomeric compounds.

The LIFT printing was also studied for the enzyme luciferase as a further biogenic material [77]. The enzymatic activity of luciferase is part of the chemical cascade of the *in vivo* bioluminescence of fireflies. A visible luminescence is emitted when luciferase reacts with the substrate luciferin in the presence of oxygen and adenosine triphosphate (ATP). A simple microsensor device for ATP microanalytical detection was fabricated, where, via the LIFT printing process, luciferase pads were deposited in prefabricated 40 μm deep cavities of a polydimethylsiloxane

(PDMS) chip on top of an integrated microphotodiode that can detect quantitatively the emitted luminescence. The third or fourth harmonic emission of a Gaussian Nd:YAG laser (355 and 266 nm, respectively, with 10 ns pulse length) were used with a focus spot of 100–300 μm at 2J cm^{-2} laser fluence. For the deposited luciferase spots, a good adhesion was found on the PDMS surface. The bioactivity of the luciferace patterns transferred on the PDMS chip was investigated by reacting the enzyme with ATP and luciferin. Patterns transferred at 266 nm showed no luminescence activity, indicating that the enzyme functionality was not preserved under these conditions. However, spots transferred at 355 nm exhibited a yellow chemoluminescence, which showed almost identical spectrophotometric plots as not-transferred luciferase films. Therefore, it can be concluded that bioactivity is not seriously diminished during the transfer process. Measurements of the photocurrent produced in the on-chip photodiode by the luminescence reaction with ATP/luciferin test mixtures allowed the derivation of curves fitting to the classic quasi-stationary-state enzyme kinetic equations according to the Michaelis–Menten model, and therefore a quantitative correlation necessary for a potential ATP-sensing microdevice.

Since the traditional LIFT process involves a direct exposition of the entire transfer material to the applied laser radiation, the method bears some crucial intrinsic restrictions concerning the properties of appropriate materials that have to tolerate a strong heat load. Thermally induced effects such as phase transitions and thermomechanical strain, as well as photochemical processes, have to be considered. For the LIFT deposition of metals, their thermoconductive properties, melting behavior, and surface tension of formed droplets have an influence on the morphology of deposits. The absorption coefficient at a given wavelength defines the permeation depth of the laser radiation within the material. Normally, smooth metal surfaces have a high degree of reflectivity, and therefore only a minor part of the applied laser photons is finally absorbed in a coating layer, whereas other materials have only a weak absorbance or are even nearly transparent to the incoming laser, so that thick layers are necessary for an efficient interaction with the laser. While evaporated metals can recondense again to atomic lattices, materials with high molecular weights, such as polymers or biogenic materials, may melt on laser irradiation, but a vapor formation necessary for an effective pressure buildup for the forward ejection can only be reached by fragmentation and degradation reactions either by thermolysis or photolytical cleavage of bonds, that is, only with loss of the initial material composition and properties. Neither variations in the emission wavelengths of the lasers from the far IR to the vacuum ultraviolet below 180 nm nor the application of ultrashort pulses down to the femtosecond regime could circumvent the limitations associated with the direct laser exposure of the transfer material coating. For that reason, various modifications of the original LIFT process were developed. Most of the extensions concern setup alterations of the donor system, either by specifically adding laser-absorbing intermediate release layers or by embedding the transfer materials into an easily evaporable host matrix.

5.4.3 Modified LIFT Methods

5.4.3.1 Matrix-Assisted Pulsed Laser Evaporation Direct-Write (MAPLE-DW)

For MAPLE-DW, the transfer material is embedded in a laser-evaporable matrix system, for example, frozen solvents or organic binders, and the laser is used to vaporize the matrix. The donor substrate consists of a transparent carrier coated with a suspension or dispersion of the particulate transfer material that can be either powders or small particles, or even a suspension of biomaterials including viable cells. The working principle of MAPLE-DW is outlined in Figure 5.4.3. By choosing appropriately absorbing and volatile components for the matrix, the laser irradiation (usually in the UV range) interacts preferably with the matrix components, which are then vaporized to form the pressure necessary to propel the embedded transfer material over a gap to the receiver. The liquid–vapor phase transition behavior and ejection of thin superheated solvent films have been investigated in detail with a time-resolved laser imaging technique [78]. This approach allowed for determining the generated pressures, the achievable superheating, and the relevant timescales of the vaporization process [79].

However, there may be problems involved with a certain UV load to the matrix-embedded transfer material due to absorption selectivity issues. Depending on the grain size of particulate systems dispersed randomly within the matrix, a high local resolution for depositing accurate patterns might also be restricted. Further, compared to the metal donor films in classic LIFT setups, MAPLE-DW donor films have typically a thickness of some micrometers, and if components of the thick matrix are co-deposited there may appear problems with contamination of the transferred systems. As a photodegradable polymeric matrix material, poly(butyl methacrylate) was used, which tends to decompose into its monomer units when exposed to UV irradiation below ~250 nm wavelength.

MAPLE-DW was originally developed as a method to rapidly prototype mesoscopic passive electronic device components, such as interconnects, resistors [80], and capacitors [1, 2, 81–84]. However, to obtain the functionality of the particulate materials after deposition, often posttransfer processing steps are necessary to obtain device compatibility, such as laser sintering, thermal annealing for the bonding

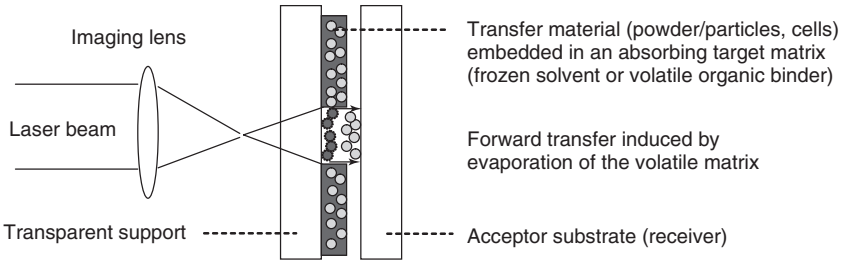

Figure 5.4.3 Working principle of matrix-assisted pulsed laser evaporation direct-write (MAPLE-DW).

of conductive powders, and especially laser trimming of blurred deposit borderlines in order to get clear-cut structure edges [85]. A series of microcircuit demonstrator devices were fabricated to study the electronic properties of such laser-deposited submillimeter-sized passive device components, such as spiral inductors [86], fractal antenna, oscillators made of resistive elements, and microcapacitors [2, 44, 87]. Two types of chemical sensors, surface acoustic wave (SAW) mass transducer and chemiresistor devices were also fabricated by MAPLE-DW of a chemoselective polymer (SFXA, a fluoroalcoholpolysiloxane), and polyepichlorhydrin (PECH), respectively [88]. Frequency response of MAPLE-DW and spray-coated SFXA SAW resonators were quite similar when exposed in on–off cycles to the nerve agent simulant dimethyl methyl phosphonate (DMPP) as test compound.

The use of a ''liquid transfer vehicle'' as the matrix for inorganic transfer material powders was applied to add micropower storage devices onto printed circuit boards (PCBs). Planar alkaline as well as lithium-ion microbatteries were fabricated by applying correspondingly composed inks in the MAPLE-DW process [89, 90]. In a similar manner, colloidal TiO_2 pastes were used in donor substrates to create on-chip PV microdevices based on dye-sensitized solar cell technology [91].

For the deposition of biogenic materials, MAPLE-DW contributed to the progress in the fabrication of biodevices and sensors [92]. Solutions or suspensions of active proteins, including enzymes and antibodies, could be laser deposited by this method, and evidence for the conservation of the biologic activity of these materials after transfer has been demonstrated [93]. Test assays consisting of microarrays with different immobilized proteins were fabricated and their specific antibody–protein binding capacity was checked by staining with fluorescently tagged complementary proteins.

For the fabrication of more demanding devices with delicate biomaterials such as proteins and living cells, MAPLE-DW has been proved a promising approach for LIFT deposition [94]. For the fabrication of the donor substrates, the biologic materials were trapped at low temperatures in a frozen matrix of appropriate solvents [95]. A series of studies were carried out with 193 nm ArF excimer lasers since most organic compounds absorb strongly in the short UV range below 200 nm [92, 93]. Therefore, the propagation depths (i.e., the optical length) of the laser can be kept small, and only a small layer of the coated entire donor target is destroyed by the laser radiation to deliver the propellant for the rest of the overlying donor biocoating. However, most of the biologic materials do not tolerate corresponding laser-absorptive organic solvents, but water as a completely biocompatible solvent has no strong enough absorption coefficient at 193 nm, so that the UV light can pass through the frozen biomatrix layer and damage the embedded UV-sensitive species. In order to circumvent the problem of low absorption of a frozen water matrix, UV-absorptive water-based biocompatible matrix media systems were tested (e.g., Dulbecco's Matrigel^{TM}), which contribute to the volatilization of the biolayer on rapid laser heating and form a vapor pocket that provides the thrust for the catapulting process [96]. This approach allowed transferring, for example, living rat cardiac cell arrays and stacks into a biopolymer matrix with near-single-cell resolution. In addition, patterns and even three-dimensional structures of living

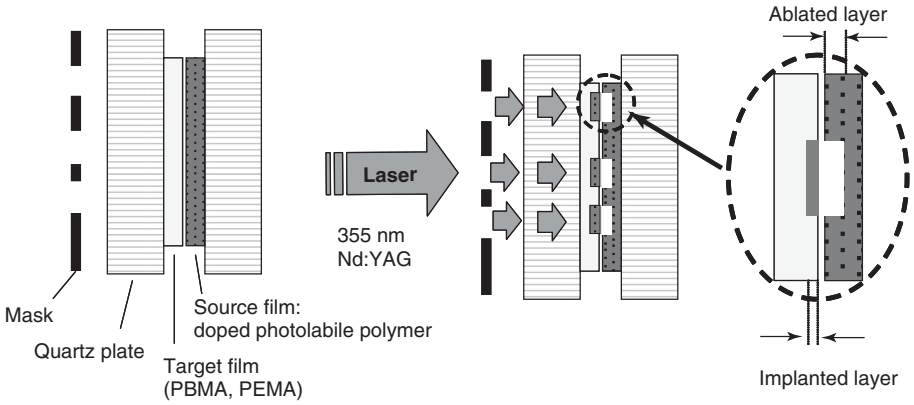

Figure 5.4.4 Scheme for laser molecular implantation (LMI) PBMA, poly(butyl methacrylate); PEMA, poly(ethyl methacrylate).

cells have been formed by MAPLE-DW. Various eukaryotic as well as prokaryotic cells grown in a corresponding culture medium matrix were transferred with the pulsed laser onto the receiver surface. Depending on the size of the focus area small cell groups from the culture could be optically selected and accurately deposited as patterns of dissected individual cell conglomerates. Bioassays and fluorescent protein marking demonstrated a high degree of viability of the cells after laser transfer into appropriate growth media. Tailored codeposition of various cell types allows not only applications for tissue engineering but also the integration of combined native cells for the fabrication of biosensor and detector devices.

5.4.3.2 **Laser Molecular Implantation (LMI)**

A further technique for the laser transfer of molecular compounds is LMI. The scheme of LMI is shown in Figure 5.4.4, and illustrates a certain correspondence to the setup for VPLD as depicted in Figure 5.4.2B. For LMI, a laser beam, which may be shaped by a mask, passes through a transparent substrate coated with only a weakly absorbing polymer layer (the target film as e.g. poly(butyl methacrylate), PBMA, or poly(ethyl methacrylate), PEMA) that is in contact with an absorbing polymer film containing the molecules that should be implanted, for example, fluorescent probes such as pyrene [97–99] or photochromic molecules [100].

The laser then decomposes preferentially the absorbing polymer matrix into small fragments, resulting in a pressure jump that assists the implantation of the embedded probe molecules into the nonabsorbing polymer film. A highly UV absorbing and distinctly photolabile triazene polymer used as the absorbing polymer matrix of the pyrene-doped source film on laser irradiation at 355 nm decomposes in a defined manner into small volatile fragments [101]. It was possible with this approach to implant pyrene with a resolution given by the mask into the target polymer with a depth of some few tens of nanometres. The disadvantage of this method is the limited number of available polymers with a high transparency and a quite low glass transition temperature T_g. A low T_g

makes the implantation of the transferred molecules more efficient because of a controlled softening of the target film by a heat-induced phase transition triggered by the pulsed laser irradiation. However, implantation was only possible with a maximum depth <100 nm. In later studies, phthalocyanine [102] and coumarin C545 and C6 were implanted in an analogous manner, and in the process now called *laser-induced molecular implantation technique* (LIMIT) [103, 104].

5.4.3.3 Layered Donor Systems with Intermediate Absorbing Films

Again, progress in the development of LIFT-based material deposition techniques was stimulated by process optimization in printing applications. The very first LDW image recordings used mostly black pigments and dyes for printing purposes, which were directly compatible with the use of IR solid-state and diode lasers because of their corresponding inherent strong absorption. However, laser-absorbing black pigments, such as carbon black, graphite, and metal oxides, which work as black body absorbers in conjunction with common near-infrared (NIR) lasers, are not compatible for printing other colors. To enhance the interaction of the laser with the imaging medium layer on a color donor sheet, ''colorless'' IR-absorbing dyes with substantially no absorption in the visible area were used as colorless sensitizers. Such IR absorbers convert the laser light to thermal energy and transfer the heat to the colorant imaging layer, which then gets ablated and transferred to the receiving element. The laser-induced ablation-transfer imaging process entails both complex nonequilibrium physical and chemical mechanisms. The ablation transfer is triggered by the rapid and transient accumulation of pressure within or beneath the mass transfer layer, initiated by laser irradiation. Various factors contribute to such a laser-triggered pressure accumulation, such as rapid gas formation via chemical decomposition combined with rapid heating of trapped gaseous products, evaporation and thermal expansion, and, in addition, propagation of shockwaves. The force produced by the immediate release of such pressure has to be sufficient for a complete transfer of the exposed area of an entire layer rather than the partial or selective transfer of components thereof. This is the particular difference of laser ablation transfer (LAT) from other material transfer imaging techniques based on equilibrium physical changes in the material, such as thermal melt transfer and dye sublimation-diffusion thermal transfer, where laser-addressed local heating is also employed. For all techniques, the formulation of the ink with an appropriate binder system plays an essential role. For thermal melt transfer applications the composition must contain low melting binder materials, whereas for laser-ablation transfer imaging the binder needs to consist of easily heat-decomposable and thermolabile components that form volatile degradation products when heated.

Former laser imaging recording processes that use self-oxidizing binders in conjunction with black absorber pigments as light-to-heat converting initiator components that trigger the blow-off reaction have already been mentioned in Section 5.4.2.1.1. As a further development, in 1992 a patent disclosed the combination of efficiently thermocleavable polymer binders doped with colorless IR ablation sensitizers as thermotriggered release system for LAT color imaging [105].

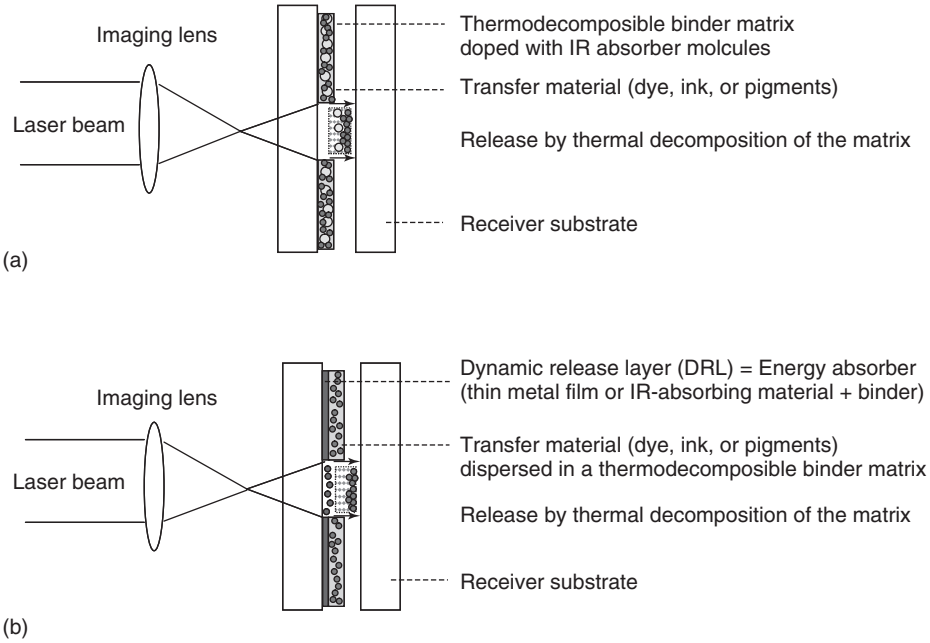

Figure 5.4.5 Scheme for laser ablation transfer imaging. In setup (a), the infrared absorbing compounds are formulated together with the coloring agents into the same binder matrix, forming a single-donor coating layer. The IR ablation sensitizers convert the near-infrared laser radiation into heat within the entire film. For setup (b), a thin intermediate metal layer is added between the carrier and the imaging coating that partially absorbs the incoming NIR radiation. Owing to its higher absorption the metal layer acts as an efficient thin-film heat converter that deposits the thermal stimulus for the decomposition of the overlying color coating in a much smaller volume close to the substrate interface, enabling a more defined ablation transfer behavior already at lower threshold fluences.

Tailor-made, thermocleavable polycarbonates and polyurethanes with low equilibrium decomposition temperatures around 200 °C were used as the binder, which was doped with Cyasorb^{TM} IR 165 dye as the IR-absorbing sensitizer. To this functional binder matrix, commercial gravure color ink formulations containing, in addition, nitrocellulose as a self-oxidizing component, were added. Absorption of IR laser radiation by the ablation sensitizers causes a local heat accumulation that initiates the decomposition of the thermolabile binder matrix together with the ignition of the blow-off reaction of the self-oxidizing binder compound. The principle of LAT imaging is outlined in Figure 5.4.5a. Both the imaging dye composition and the IR ablation sensitizers are homogeneously formulated within the heat-degradable polymeric binder matrix, forming a single donor layer. On IR laser exposure, the binder matrix decomposes into small evaporable fragments that build up the local transient pressure to propel the imbued colored agents toward the receiver sheet.

The mechanism of LAT was investigated in detail by time-resolved ultrafast microscopy, where propelling speeds of the ejected coating of at least Mach 0.75 were observed [106]. With an optical absorption coefficient α of about 12 000 cm^{-1} at 1064 nm for such a typical color coating, the optical propagation length $1/\alpha$ of the lR photons within the absorbing layer is in the range of ~850 nm, which is in the same dimension as the donor layer thickness of around 1 μm useful for LAT imaging applications. A model calculation for such an absorber-sensitized system resulted in estimated heating rates dT/dt as high as 10^9 °C s^{-1} and an ablation temperature above 600 °C for transient nonequilibrium superheating conditions during laser irradiation. When the coating material was irradiated above a well-defined threshold fluence of around 60 mJ cm^{-2}, essentially complete material transfer occurred provided that the pulse duration is shorter than ~200 ns, the time interval required for substantial heat transfer into the substrate. LAT made it possible to produce high-resolution full-color graphic images at comparably high printing speeds, demonstrating its potential as a versatile dry mass transfer method for also printing functional materials in direct-to-circuit-board device fabrication applications.

5.4.3.3.1 Laser Ablation Transfer (LAT) with a Metallic Release Layer

A significant improvement in the LAT process could be achieved by a further modification of the donor substrates, according to Figure 5.4.5b. The original LAT setup for color imaging applications uses organic NIR absorber dyes as ablation sensitizer dopants for the heat generation within the irradiated coating (corresponding to Figure 5.4.5a). Since only a certain maximum dopant concentration can be added to the binder matrix beside all other essential components, the NIR absorption of the whole coating stays rather small, even when the IR dyes themselves have a high specific absorption. As a consequence, the incoming NIR photons can propagate far into the coating until they are quantitatively absorbed, so that comparably thick coatings are necessary for a complete absorption of the laser radiation, and the LTHC process runs distributed within the whole film thickness. As already mentioned in the section on LIFT of metal films, metal absorption properties are in general superior to other material classes because of their characteristic electronic structure that allows optical excitation with high yields and in a wide spectral range. However, the absorption coefficient α is wavelength dependent and usually smaller for NIR radiation compared to UV excitation. While near-UV radiation is completely absorbed usually in a thin skin layer of some tens of nanometres (e.g., ~10 nm for Al at 308 nm, corresponding to an absorption coefficient of ~10^6 cm^{-1}) [107], NIR radiation has a slightly higher penetration depth in the range up to ~50 nm. But even when metals have a high absorption, they have at the same time a high degree of inherent reflectivity that causes crucial losses by back reflection, which is a disadvantage at least with respect to the high cost of laser photons. Nevertheless, thin metal layers can act as efficient light-to-heat converters, which can also be easily ablated and vaporized with a high relative increase in volume.

The improved LAT donor films include a thin metal film as a DRL, as outlined in Figure 5.4.5b. An ultrathin vapor-deposited aluminum film layer with a thickness

of only ~3 nm was used in the first study on the effect of such a metallic interlayer on the LAT imaging process [106]. Such an ultrathin Al layer represents a partially transmitting and partially absorbing interlayer (apart from the inherent reflection losses mentioned above). With stationary low-intensity irradiation at 1064 nm, such films show a reflectivity of ~27% of the incident light, a transmission of ~33%, and therefore a fraction of absorbed light of about 40%, which corresponds to an absorption coefficient α of about $3 \times 10^6 \mathrm{cm}^{-1}$ at 1064 nm. However, all these values may be affected dramatically during pulsed laser irradiation due to temperature effects and phase transitions induced by ultrafast superheating, but with such a thin DRL, the threshold fluence for ablation is reduced by nearly 50%, and the ablated spots show a better shape. The ablation mechanisms involved in the DRL-assisted LAT process are complex, since the thin metal film itself absorbs only a part of the incident radiation, whereas the remaining part gets absorbed by the coating layer containing an IR sensitizer dye. Therefore, LTHC takes place within both layers, resulting in rapid heating of the metal DRL, which helps to reach the decomposition temperature necessary for the ablation of the thermolabile polymer binder matrix within a much more confined part of that layer close to the carrier interface. Hence, the transient pressure jump is generated more efficiently and more localized in a substantially smaller volume, which leads to a more controllable propulsion, and, finally, to a more homogeneous ejection of the overlying coating. Since the ultrathin DRL has a much higher absorption coefficient α compared to the sensitizer dye-doped coating, the LTHC process on a laser pulse results in a completely different temperature profile along the thickness of the overlying coating if the DRL is present. The threshold temperature for ablative decomposition is reached earlier and in a more confined zone so that the ejection process starts before the thermal diffusion during the pulse length reaches the top surface of the overlying coating. Therefore, a part of the coating stays ''cold'' (i.e., preserved from phase changes) and even shielded from the incident laser irradiation and can be propelled off without severe modifications.

Time-resolved ultrafast optical temperature measurements were performed for the DRL-free LAT imaging film exploiting the ''molecular thermometer'' of the IR absorber dye Cyasorb IR-165, which changes its absorbance coefficient in the visible range linearly with increasing temperatures [108]. The time-dependent transmission at 633 nm was measured at the onset of ablation triggered with the 1064 nm laser, and the peak temperature of the doped binder just before LAT starts was found to reach about 600 °C [109]. This is somewhat less than the melting temperature of aluminum (660 °C), and, indeed, electron microscopy inspection of ablated spots of donor films with an intermediate aluminum DRL showed that the Al metal film itself was not completely ablated, even when the metal layer obviously was temporarily molten, but not substantially vaporized. This can be attributed to the higher absorption coefficient of the thin metal film, which then acts more efficiently as a confined LTHC layer that creates a local hot spot that overshoots the thermochemical decomposition temperature for ablation of the thermolabile binder. A later study by secondary ion mass spectrometry (SIMS) analyses of the transferred pixels on the receptor surface revealed that aluminum residues are codeposited

with the imaging inks. This finding is consistent with the observed phase transition of the remaining spots of the aluminum DRL on the donor after irradiation.

Also, already in 1993 the same authors reported a study on the effects of laser pulse length in the LAT process. Instead of 150 ns pulses of a common solid-state laser, they used 23 ps duration pulses generated by a Kerr lens mode-locked (KLM) 1064 nm laser [110]. It was found that the threshold fluence of ablation for donor film systems with a DRL of aluminum was reduced to 1/10th of that observed with nanosecond pulses (i.e., from 80 to 8 mJ cm^{-2}). Using the immense instantaneous peak powers of picosecond duration pulses, ablation can be induced at a lower fluence through vaporization of the thin Al interlayer. Vaporization of the metallic layer is intrinsically a more effective ablation method compared to the ablation of polymeric binders, because the relative increase in volume on vaporization is considerably larger (due to ''atomization'' of the metal layer) than for organic coating materials. The heating rates dT/dt of the Al layer observed with the picosecond laser were on the order of 10^{14} °C s^{-1} (i.e., about 5 orders of magnitude higher than for nanosecond pulse irradiation). Therefore, with respect to the ultrashort timescale of optical heating, heat diffusion effects via thermal conduction to the adjacent carrier and coating material within the irradiated spot are much less relevant, and the Al layer can reach and exceed the boiling point of Al, 2467 °C, already at low fluences just below the ablation threshold. The spatial distribution of heat in the dimension along the axis of propagation of the laser pulse differs essentially from the heat profile generated by about 1000 times longer nanosecond laser pulses with the same power density, where temperature losses by heat diffusion prevent the Al layer from immediate vaporization.

A similar color printing technique called *laser thermal transfer* was described, which is based on laser heating performed with 100 mW diode lasers with an emission wavelength of 825 nm and used in a modulated pulsed manner with tunable pulse durations in the range up to tens of microseconds [111]. For the donor ink sheets, a 1.8 μm thick light-absorbing layer consisting of an NIR absorber dye (a commercial bisaryl nickel complex, PA-1006 by Mitsui Chemicals Inc.) with a λ_{max} at 870 nm dispersed in a polycarbonate binder matrix was coated on top of a transparent base film, in close analogy with Figure 5.4.5b. As the coloring layer, sublimation dyes with melting points around 150 °C were coated by vacuum evaporation. Depending on the exposure time defined by the individually modulated pulse duration, increasing amounts of the sublimation dyes were deposited, when the donor film and receiver medium are in contact. Laser beam spots with a diameter of 25 and 3 μm were used to print image structures, and a resolution of 2540 dpi (corresponding to a single dot size of about 10 μm) has been reported. However, with a transfer gap of 25 μm between the donor and receiving sheet, a threshold pulse length of more than 30 μs was necessary for a transfer of the ink layer. Obviously, it needs a certain time with a given heating rate to obtain the critical temperature level for an ''explosive'' release mechanism similar to the LAT imaging systems with thermolabile binders, even if the timescale of laser exposure is in the multimicrosecond order, and both mechanisms, dye vaporization and ablation, may contribute to the transfer.

An evaporated black aluminum DRL in combination with an additional layer of an energetic polymer is claimed in a US patent for printing applications, and called *laser propulsion transfer* [112]. Mixed oxides of aluminum were vapor coated onto a carrier film as the DRL. On laser-induced heating, the black aluminum is exothermically oxidized to Al_2O_3, which is colorless, and serves at the same time as the initiator for the decomposition of the energetic polymer coating. The use of thermolabile gas-generating decomposing materials in conjunction with a laser-absorbing DRL allowed improving the efficiencies and speed of the printing process. Gas-producing polymers are known, for example, as energetic components of solid rocket propellants. Such polymers are composed of repeating units with nitrogen-containing precursor groups (such as azido, nitro, or triazole moieties), which on heat exposure can split off molecular nitrogen gas (N_2) during thermal decomposition, resulting in a significant volume expansion by the formed gaseous products. If such gas-producing polymers have a thermally available nitrogen content greater than about 10 wt%, they can serve as excellent propellants for thermal mass transfer operations. Examples of such energetic polymers, which exothermally decompose and form a large amount of gaseous products when heated above a certain threshold temperature on the millisecond or microsecond scale, are glycidyl azide polymer (GAP), poly[bis(azidomethyl)]oxetane (poly-BAMO), and polyvinylnitrate (PVN). Chemical structures of some nitrogen-rich polymers are shown in Figure 5.4.7. Such polymers were also studied in designed solid fuel tapes for diode laser-driven microthrusting devices for the propulsion and steering of ultralightweight minisatellites [113–115]. Owing to the involved exothermal decomposition processes, only low laser power densities are necessary to ''ignite'' the blow-off reaction, and therefore comparably high writing speeds of more than 50 m s^{-1} are possible with focused spots of common IR lasers on appropriate drum printing systems with galvanometric scanners. However, since most printing processes are performed in a direct-contact mode, it is difficult to differentiate whether the heat-induced mass transfer process corresponds to a LIFT mechanism or rather to a melt-type thermal transfer printing method with the laser as the fast-performing point heat source. Nevertheless, with the upcoming high-power semiconductor laser sources, new optical printing heads for miniaturized high-definition digital imaging applications based on laser-induced thermal transfer systems have been developed with printing resolutions above 3000 dpi [116–118].

5.4.3.3.2 **Inorganic Materials as Absorbing Release Layers**

A different concept of a laser-absorbing layer that contains volatile atoms that can be immediately released on laser heating was used to transfer 100 nm thin Al films. Hydrogenated amorphous silicon (*a*-Si:H) films formed on UV transparent quartz substrates were irradiated with 308 nm pulses of a XeCl excimer laser [119]. Films with a thickness of 50 nm and with a concentration of hydrogen atoms of 10 at.% were used as laser-responsive DRL, which transferred the top-coated Al layer at a laser fluence of 200 mJ cm^{-2}. When the *a*-Si:H-film is rapidly heated during the laser irradiation, the internally trapped hydrogen is liberated by explosive effusion

and provides by adiabatic expansion the pressure for the propulsion of the Al film. With respect to device fabrication applications, microstructured arrays of Al metal lines were deposited by preparing corresponding mask-patterned targets with a target–receptor separation of 125 μm. However, similar to direct LIFT of aluminum and other metals, the transferred Al structures also show some irregularities by splashing and splattering when transferred by the hydrogen-assisted LIFT method. Cleaner transferred features were observed when this method was used to deposit Si structures directly obtained by fully laser melting the entire *a*-Si:H propellant films at higher fluences [120–122].

5.4.3.3.3 Metal Films as Absorbing Release Layers

The interaction of short-pulse laser radiation with metals causes a complex cascade of dynamic nonequilibrium excitation processes that finally lead to the thermalization of the absorbed laser light. Absorbed laser photons excite the conducting band electrons with subsequent energy relaxation, that is, the energy transfer from the hot electrons to the lattice vibrations due to the electron–phonon interactions and the electron heat conduction from the irradiated surface to the bulk of the target [123]. The propagation depth of the incoming laser photons in metals is small only because of the high (wavelength-dependent) absorption coefficients $\alpha(\lambda)$ and covers generally only a skin depth of some tens of nanometers or less. Depending on the electronic structure of the individual metals, the thermophyiscal properties, including their temperature-dependent changes, differ crucially, which has to be carefully taken into account for the design of sophisticated laser ablation applications. A dominating effect has the strength of the electron-lattice energy exchange, that is, the electron–phonon coupling that defines the temperature-dependent electron relaxation times. An electron–phonon coupling factor G has been derived from theoretical calculations and pump-probe experiments that reflect some aspects of the different ablation behavior of various metals in addition to their different physical properties, such as density, melting and boiling temperatures, heat capacity, as well as thermal and electrical conductivity. A high value of the electron–phonon coupling factor reflects an efficient energy transfer from the excited electrons in a nonequilibrium thermal distribution to the lattice. The finite time for the energy equilibration with the metal lattice is called the *electron–phonon relaxation time* τ_c. For metals with high values of the electron–phonon coupling factor G, the corresponding relaxation (or thermalization) time τ_c is shorter than for metals with low G values, with a typical range of τ_c between 0.8 ps for gold and 0.05 ps for titanium. For laser pulse durations shorter than the thermalization time τ_c, the electron distribution in the irradiated metal layer is a nonequilibrium state with a transient electron temperature much higher than the lattice temperature. Therefore, with appropriate femtosecond pulse durations below the corresponding τ_c, metals can be ablated in a much more controlled manner since side effects caused by thermal conduction are much less prominent compared to longer pulse durations where a heat transfer to the metal lattice takes place. Table 5.4.1 compiles characteristic thermophysical properties of some metals typically used as absorbing DRLs.

Table 5.4.1 Relevant thermophysical properties of some representative metals used as absorbing DRL [51, 123].

	Aluminum (Al)	Gold (Au)	Chromium (Cr)	Titanium (Ti)
Electron configuration	$3s^2 3p^1$	$5d^{10} 6s^1$	$3d^5 4s^1$	$3d^2 4s^2$
Melting temperature (°C)	660	1063	1875	1668
Boiling temperature (°C)	2450	2970	2665	3260
Thermalization time τ_c (ps)	0.55	0.8	0.1	0.05
Skin depth (nm)[a]	15	4	9	19
Electron–phonon coupling factor G (10^{17} W m^{-3}K^{-1})[b]	2.45	0.3	4.2	~130

[a] For 800 nm irradiation.
[b] At room temperature.

The electronic structure of the metals contributes to the thermophysical properties. It has obviously an influence, whether the electron configuration corresponds to a free electron gas model or if the d bands of transition metals are almost filled or less than half filled. The strength of the electron–phonon coupling depends on the electron temperature, and can either increase (Al, Au, Ag), decrease (e.g., for Ni, Pt), or exhibit nonmontonic changes (Ti) with increasing electron temperature [123]. Therefore, the strong temperature dependencies of the electron–phonon coupling have to be taken into account in the interpretation of experimental data obtained under conditions when the transient values of the electron temperature undergo significant variations, as this is undoubtedly the case during laser ablation and LIFT conditions.

Gold films with a thickness up to 500 nm were tested in a LIFT study for the transfer of the laser dye Rhodamine 610 on SiO_2 substrates with the second harmonic emission at 532 nm of a Nd:YAG laser [65]. In the same study, the laser dye was directly transferred without an intermediate metal layer, as already mentioned in Section 5.4.2.1.3. Measurements of the fluorescence activity were used as an indicator for conservation of the dye functionality. Best results with respect to the fluorescence intensity after LIFT deposition of dye spots with a diameter of about 200 μm were obtained with a thickness of the base gold film of 50 nm and in vacuum and with a rather low laser fluence of ~50 mJ cm^{-2}. Under these conditions, the gold film is about two to three times thicker than the estimated optical absorption length (the so-called skin depth) of around 20 nm for 532 nm irradiation. Thicker gold films needed higher fluences for ablation, and the transferred laser dye on the acceptor substrate was found to have a less intense fluorescence response and was covered by evaporated gold. When the transfer was carried out in vacuum, the results were significantly better compared to experiments in ambient atmosphere, and the shape and morphology of the deposited spots were much more defined.

In combination with fast-imaging techniques, the laser-induced fluorescence of gold atoms was also used to visualize the time-resolved dynamics of the ejection process during LIFT propulsion [124]. Thin gold films (20, 100, and 500 nm in thickness) evaporated on fused silica substrates were irradiated by a pulsed dye laser at 440 nm (~9 ns pulse width), and the temporal and spatial distribution of the ablated species from the film were observed by imaging of the fluorescence emission at 627.8 nm after excitation by a probe laser beam (268 nm). In vacuum, the velocity of an ejected cloud of vaporized gold atoms exceeds 2×10^3 m s^{-1}, whereas emissive particles or droplets reached a speed of around 100 m s^{-1}. When an acceptor substrate was placed in front of the donor film at a distance of either 70 or 500 μm, a reflection of the ejected species was observed. This indicates that the conditions of the mechanical impact also play an essential role in the LIFT deposition process, and the velocity of the collision of the catapulted flyer with the receiving surface has to be optimized in order to get sufficient adhesion. Owing to the gas resistance under atmospheric conditions, the ejection speed is slower, but always accompanied by a shock wave in the gas phase, which may cause similar detrimental effects when reflected at the receiver surface (Section 5.4.3.3.6).

Red and green phosphorescent powders were deposited by the DRL-assisted LIFT method with a KrF excimer laser (248 nm emission, 25 ns pulses) using an intermediate 100 nm thick sputtered gold film [125]. In order to form a donor layer of the phosphorescent powders on top of the basic gold release layer, they were coated according to the concept of MAPLE-DW mentioned in Section 5.4.3.1 as a suspension (with glycerol and isopropanol as the solvents) by electrophoretic deposition, resulting in a wet viscous powder layer with a thickness of ~10 μm. On irradiation, the absorbing gold layer gets vaporized and the powder suspension with the high-boiling glycerol is catapulted over a gap of 25 μm onto the receiver. Interdigitating pattern arrays of green and red fluorescent powder deposits with a diameter of ~50 μm each were deposited and their emission spectroscopically characterized by cathodoluminescence (CL) measurements. The emission spectra of the transferred powder were identical to the corresponding CL measurements of the donor layer. The conservation of the functionality and the precise deposition of light-emissive materials as small pixels are of general interest for color screen and display device applications. However, there might be some technical restrictions for this approach for potential device integration since the transferred spots are obviously contaminated with codeposited small gold droplets that might impair the device performance.

In order to circumvent the codeposition of the metallic release layer, a modification of the MAPLE-DW process has been reported for the deposition of phosphor pastes by laser heating [126]. Instead of a thin metal film, a 200 μm thick stainless steel sheet is used, on which arrays of hemispherical blind holes with a diameter of 300 μm were etched. These cavities were filled with a viscous paste of the phosphorescent powders and served as locally resolved donor dots for the LIFT process. The binder matrix consisted of ethyl cellulose and organic solvents with boiling points between ~120 and >200 °C. On laser exposure of the back of the steel sheet, the powder mixture gets ejected because of the fast evaporation and

bubble formation of the superheated solvents that form a jet. With the appropriate paste composition and laser heating conditions the stream of the phosphor paste is ejected as a spray, which is deposited as a regular plaque onto the receiver. This specific LIFT modification has been named *laser-induced thermal spray printing* (LITSP).

Thin metal films were also introduced as laser-absorbing layers in donor systems for the transfer of biomaterials. The requirement of strictly biocompatible matrix systems and the weak absorption of water-based matrix media has been mentioned in Section 5.4.3.1. With respect to the short propagation depths of UV laser photons in a metal layer (the so-called optical skin depth), only ultrathin absorbing interlayers of 35 nm for gold and 75 nm for titanium were found to be necessary as efficient energy conversion layers for the gentle transfer of various biomaterials embedded in common water-based matrix media with a frequency-quadrupled Nd:YAG laser (266 nm) [127]. Also, 85 nm thick films of biocompatible TiO_2 as UV-absorbing compound had the same effect of preserving the biomaterial from direct laser interaction and of providing a rapid LTHC that contributes to the fast vaporization of the adjacent part of the overlying water-based biomatrix to build up the catapulting pressure. By choosing the appropriate combination of laser fluence, pulse duration, and film thickness the propagation of the laser photons stays restricted to the optical length within the metal layer, whereas the generated heat can propagate (i.e., the thermal penetration) without further significant ablation into the much thicker aqueous biofilm causing local vaporization. By that, the ejection process for the transfer includes a different forward-ablation mechanism, which is more in analogy with the IR-absorbing light-to-heat converting DRL systems discussed in Section 5.4.3.3.1. Instead of the ablation of the entire donor film, a forward jetting of the viscous biomatrix is achieved, which allows a more precise deposition of droplet-like features. In a series of papers, this method was referred to as *''biological laser printing''* (BioLP^{TM}) [128] and the adjacent deposition of multiple cell types and accurate large-scale cell arrays are demonstrated, useful for potential applications in biodevice and minisensor fabrication as well as for tissue engineering [129].

Radiation-absorbing titanium layers of about 50–60 nm thickness have been also used in a LIFT setup to successfully deposit droplet-like microbumps of viscous DNA dispersions with the 355 nm emission of a frequency-tripled Nd:YAG laser [130]. The same setup was then also used for the precise spotting of microdroplet arrays of a purified bacterial antigen, which conserved its immunological reactivity after having been transferred [131]. For biodevice fabrication, where tiny amounts of delicate materials have to be manipulated, this modified LIFT approach opens up a promising orifice-free and noncontact deposition technique for the gentle and accurate direct-write of ''bioinks'' [132–134] with appropriate rheological properties for droplet formation during the laser-triggered jetting process [135–141]. The experimental results with an intermediate metallic absorption layer are clearly superior with respect to droplet morphology and resolution to an earlier approach called *light-hydraulic effect* (LHE), where viscous black printing inks were similarly forward ejected by direct IR laser exposure [142].

A series of bio-LIFT experiments were also reported with ~50 to 100 nm thick silver layers as radiation absorbers in conjunction with 248 nm pulses (30 ns duration) of a KrF excimer laser, and referred to as *absorbing film-assisted laser-induced forward transfer* (AFA-LIFT) [143]. Without an embedding matrix, dried conidia of the fungi *Trichoderma* were transferred over a gap of 1 mm in a laser fluence range between 35 and 355 mJ cm^{-2} [144]. Various mammalian cell types were tested with this LIFT approach, which survived the transfer process even when acceleration of the cells in the jetted droplets reached approximatively $10^7 \times g$ [145, 146]. It was observed that for all fluences above the transfer threshold the silver layer was completely ablated, leaving a transparent hole on the donor substrate. Therefore, it has to be assumed that silver residues are codeposited together with the biomaterial. Even when first microscopic inspections revealed obviously no visible metal droplet contamination of the deposited biospecies, submicrometer-sized Ag particles (250–700 nm) have been detected later in a more detailed study on the amount, size, and local distribution of such metal precipitations [147]. Since it is well known that dispersed silver particles have distinctly biocidic effects, such codeposited residues of the metallic absorber layer may restrict the viability or functionality of transferred biomaterials, for example, in biosensor devices.

Ejection of biomaterial-containing microdroplets onto bioassay chips was recently studied with absorbing ultrathin (10 nm) gold layers with 15 ns and 500 fs pulses of a 248 nm excimer laser system [148–150]. With the same transfer layer thickness of a viscous glycerol/phosphate-saline-buffer solution and with the same incident laser fluence, smaller droplets were deposited over a gap of 20 to 1000 μm with the femtosecond pulses. Although the threshold energy was lower for the femtosecond laser pulse transfer, both laser pulse regimes could be used for the pattern transfer with a model protein (Avidin) without significant deterioration of its functionality, as was shown by a key–lock reaction with Biotin as the complementary ligand. However, with nanosecond pulses the distance for transfer is longer than in the case of the femtosecond laser system, obviously due to a different jetting behavior. However, the size of the deposited droplets depends also on the dimensions of the laser beam, its fluence, and further, the composition of the transfer layer (e.g., the glycerol content) that influences the rheological behavior as well as the wettability of the accepting surface play an important role.

A very similar setup with 40 nm thick Cr films as the radiation-absorbing layer has recently been reported for the LIFT deposition of biotin dispersion microarrays with a 266 nm solid-state nanosecond laser system on low-temperature oxide layers on Si [151]. The influence of the chemical functionalization of the receiver surface was studied to obtain optimum immobilization of the deposited biotin droplets. Compatibilization by chemical modification of electronic semiconductor surfaces is a necessary prerequisite for the fabrication of biosensor devices. The LIFT deposition process of chemical sensing polymers onto prefabricated capacitive micromechanical sensor arrays was studied with respect to the integration of the LIFT technique for the production of real biosensor systems [152–154].

A combination of the two-photon polymerization (2PP) technique and LIFT with 55–60 nm thick gold films as energy-absorbing release layers allowed the

combined deposition of 3D scaffolds as artificial extracellular matrix together with viable cells [155]. This represents an integrated laser-based approach for the tailored fabrication of cellular tissue constructs with a microengineered polymer scaffold matrix with controlled pore design for cell deposition. Prefabricated scaffolds were then seeded with endothelial and muscle cells by the LIFT process. Cell suspensions were dispersed as ~50 μm thick layers on top of the Au-coated donor slides, and the LIFT deposition performed with single nanosecond pulses of a solid-state Nd:YAG laser at 1064 nm focused to a 45 μm diameter spot. Single droplets, each containing 20–30 cells, were ejected at a pulse energy of 66 μJ and deposited over a gap between the donor and prepared collector slide of 350 – 500 μm. The combination of well-defined laser-fabricated porous microscaled structures with accurate LIFT microdeposition methods of sensitive biomaterials might be relevant not only for fundamental studies of cell–matrix interactions but also for future tailored applications in cell-based biosensor and device engineering.

Direct LIFT deposition of thin polymer films has been proved to be unsatisfactory because of substantial chemical alteration of the transferred macromolecular materials. However, with a metallic DRL, clearly better results are reported with respect to the pixel cohesion, homogeneity, and surface roughness, even when co-deposition of metal residues could not be avoided. Effects of the thickness of gold and silver metallic DRLs and the influence of the pulse duration on the transfer performance has recently been studied again [156] for the transfer of ~300 nm thick films of the conducting polymer PEDOT:PSS, which is frequently used as an electrode-coating material in the fabrication of electronic thin-film devices. As already mentioned, direct LIFT deposition of PEDOT:PSS was tested without an intermediate absorbing DRL, and best pixel depositions were obtained only by using a UV laser. However, the conductivity of the transferred PEDOT:PSS was lost because of expected photochemical degradation reactions on direct exposure of the polymer to UV radiation. The LIFT process of films of the same conducting polymer was carried out with either 50 or 25 nm thick intermediate metallic absorber layers, and two different UV laser systems, a 248 nm KrF excimer laser with 35 ns pulse duration and a frequency-tripled Nd:YAG with 50 ps pulses at 355 nm were compared to study the influence of the different pulse durations. For the laser wavelengths 248 and 355 nm, the absorption lengths are for gold 13 and 15 nm, respectively, and for silver 15 and 51 nm. With nanosecond pulses and 50 nm Ag films, well-defined deposits are obtained. In this case, the film thickness of the Ag layer has almost the same value as the absorption length of the beam for this radiation, whereas best results for a gold release layer were obtained with 25 nm films, that is, twice the absorption length. This implies that the laser energy is converted into different metal volumes and thermophysical parameters have to be also considered. However, with the picosecond regime and gold layers, a huge amount of metallic debris has been observed all around the deposits, but they could be easily removed with a soft air blow. But SEM images and X-ray dispersive energy analyses (EDAX) show that the transferred polymer pixels are contaminated on their surface with residual nano- and microparticulate metallic debris. These

metal contaminations might be a potential drawback to the integration of metal DRL-based LIFT in electronic microdevice fabrication.

Metallic absorber layers were also used for the fabrication of small electroluminescent devices by LIFT sublimation of small light-emitting molecules in a designed vacuum chamber with a CW Nd:YAG laser [157]. The donor consists of a chromium layer sputtered onto a carrier substrate, which is then coated with the organic electroluminescent materials by high-vacuum deposition. The optical system included a highly dynamic and high-precision galvanometric scanner and allowed to achieve a focus diameter of about 35 μm on a working area of 16 cm × 16 cm. Small lines of the organic emitter materials were transferred when the focused laser beam was scanned along the back of the donor substrate, heating up locally the absorber layer. The spatially selective rapid laser heats and induces the flash sublimation of the organic molecules from the donor substrate onto the receiver substrate over a spacer-defined gap. This modified LIFT technique has been named *laser-induced local transfer* (LILT). Stripe patterns of OLEDs with a line width of ~300 μm were deposited according to a multilayered thin-film OLED device architecture consisting of a hole-blocking, an electron-transporting, and an emissive layer that was laser deposited. By optimization of the processing parameters, scanning speeds between 1 and 2 m s^{-1} were reported to achieve minimum line widths of 50–70 μm. In principle, if the deposition process is performed for red, green, and blue (RGB) emitting materials, full-color red, green, and blue organic light-emitting diode (RGB-OLED) display devices could be printed with fast processing speeds and on larger areas. However, the organic materials used need to be thermally robust to tolerate the laser-induced flash sublimation step.

5.4.3.3.4 **Laser-Induced Thermal Imaging (LITI)**

The principle of thermal imaging has been already presented in Section 5.4.3.3.1, which has been applied mainly for digital color printing. Thermal imaging enables the printing of multiple, successive layers via a dry additive deposition process at high speed and with micron-size resolution. With the ablative transfer of solid layers, the solvent compatibility issues, which are always encountered when printing sequential layers from solution, are entirely avoided. This technique has also been extended by DuPont to fabricate organic electronic devices [6], also with polymeric material sets [158]. The flexible donor sheet comprises essentially a LTHC layer (together with an optional ejection layer), which is coated with the printable electronic materials. Donor and receiver sheets are pressed together in close contact during the transfer process, which is performed by focused IR laser irradiation either from output-modulated diode lasers or scanned cw solid-state lasers. With appropriate tuning of the laser fluence and the local irradiation duration, the release layer system is thermally decomposed into gaseous products. Their expansion thus propels the top layer of the donor film onto the receiver. However, owing to inherent heat conduction processes with transient laser irradiation in the microsecond regime, the transfer material layer also gets noticeably heated, and therefore printable materials have to be reasonably heat resistant. Such a thermoimagible organic conductor was developed (a blend of

single-wall CNTs and doped polyaniline) and printed in small patterns as source and drain electrodes for TFTs. The conductivity of the deposited features depends on the applied fluence of the 780 nm IR diode laser, and decreases with increasing fluences after a maximum closely above the transfer threshold fluence. This decrease at higher fluences reflects the increasing structural degradation of the conducting polymer at elevated thermal stress. Even when this example demonstrated that components of a functioning organic electronic device can be dry printed by laser transfer, the obtained process performance proved not to be easily applicable to other material systems without refinement of the individual processing parameters and especially the material properties. From a mechanistic point of view, thermal imaging may comprise both components, fast nonequilibrium ablation processes in combination with slower equilibrium melt transfer by laser heating. DuPont has also launched a digital printing technology for manufacturing liquid crystal display (LCD) color filters that eliminates the photomasks and liquid process chemicals used in traditional photolithography. The Optilon™ TCF system [159] uses donor films for the three filter colors RGB, which are transferred and patterned on the prefabricated LCD matrix by direct laser writing. Digital files of color filter patterns are directly image transferred from the dry Optilon RGB donor films on glass substrates.

Adapted from the laser imaging and graphics applications mentioned above, 3M has developed over the past decade as an extended digital transfer method for laser thermal patterning of electronic devices, such as flat panel displays and OLED emitters. Patterning of electroactive organic materials by dry mass transfer via thermal printing techniques is intrinsically difficult because both molecular and bulk electronic properties must be preserved, even when the materials are nonvolatile or thermally labile. The 3M technique has been called *laser-induced thermal imaging* (LITI) and uses a focused CW IR laser system as a heating device in a designed exposure system with fast oscillating elliptical laser beams [160].

As outlined in Figure 5.4.6, the donor sheet consists of a flexible 75 μm thick PET support that carries the functional nontransferring layers and a top-coated ultrathin transfer layer of electronic materials. The nontransfer layers are a 1.6 μm thick absorptive LTHC layer and an additional 1 μm thick shielding interlayer. The LTHC layer is a carbon-black-based black body absorber for the applied IR radiation. The optical density and thickness of the LTHC layer are important parameters in adjusting the donor heating profile, which affects imaging quality, performance, and device efficiency. With appropriate tuning of the process parameters, heating rates up to more than $10^7\,^{\circ}\mathrm{C\,s^{-1}}$, and peak temperatures within the LTHC layer reaching from 650 to 700 °C were observed. The peak temperature within the organic transfer layer is about 350 °C, but remains above 100 °C for less than 1.5 ms. The second coated layer consists of a photocured polymer that acts as an interlayer to protect the transfer layer from chemical, mechanical, and thermal damage. The interlayer also moderates other physical defects known to arise from warping or distortion of the LTHC so that the transfer layer surface remains smooth. In addition, fine tuning of the interlayer (which may consist of more than one layer depending on the transfer layer material requirements) affects crucially

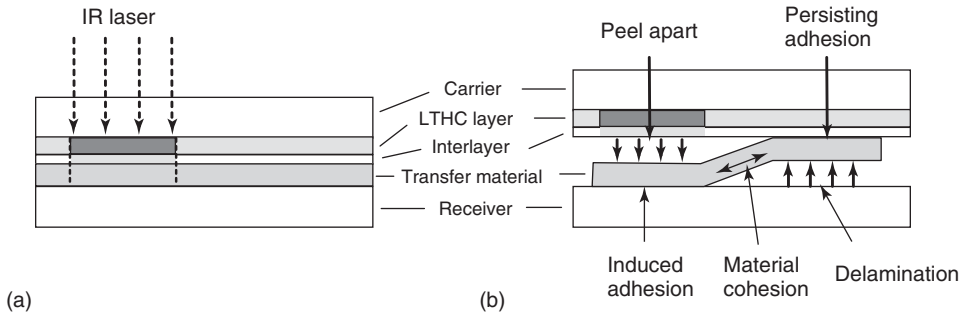

Figure 5.4.6 Scheme of the laser-induced thermal imaging (LITI) process. Donor and receiver sheet need to be in intimate contact during the mass transfer process by a thermal release/adhesion mechanism. (a) Laser irradiation of the light-to-heat conversion (LTHC) layer induces a controlled phase transition of the transfer material that leads to a local change in adhesion to the receiver surface. (b) The imaged pattern is mechanically developed by careful separation of the donor and receiver sheet.

the transfer layer release functions. Nevertheless, thermal transfer defects were observed during the LITI process of vacuum-coated OLED materials [161].

For OLED fabrication, the final coated transfer layer is commonly a thin doped evaporated emissive layer, typically some tens of nanometers in thickness. An optimal construction of phosphorescent OLED multilayer systems comprises usually a well-balanced system of charge transport and blocking layers for exciton confinement. With evaporation techniques, such stacks of multiple discrete organic layers can be deposited in reverse order on top of the interlayer on the donor sheet before the patterning step. During the LITI process, the entire multilayered stack will be transferred on the prepared receptor. A large-area laser imager with a twofold galvanoscanner system has been developed for the LITI mass transfer process with two superimposed Nd:YAG lasers focused to a Gaussian spot of 30 µm by 330 µm, delivering a laser power on the film plane up to 16 W. The optical design with fast oscillation of both elliptical beams transverse to the scan direction improves the line edge quality and precision by increasing the slope of the laser intensity profile closely above the transfer fluence threshold. Continuous variation of the scan speed and oscillation parameters such as frequency and beam dithering allow the fluence profile to be tailored to the materials and to achieve high cross-scan accuracy for writing precise line structures. Essential for good transfer results is the controlling of the thermal processes, the heat flow, and the temperature profiles from the LTHC layer to the transfer layer during the LITI transfer. A phase transition of the transfer material, for example, by exceeding the glass transition temperature T_g, facilitates the adhesion to the receptor surface. For a successful transfer, the transfer layer has to become detached from the interlayer at the same time, as outlined in Figure 5.4.6. A critical step is the separation of the irradiated donor and receiver sheet. Since there is no sharp cut or perforation along the edge of the transferred stripe, that is, along the border of exposed and unexposed donor film,

the micromechanical properties of the film during removal of the donor have a strong influence on the formation of the line edges. This is the critical region of the donor–receptor laminate where a delicate balance of adhesion and release must be achieved in order to create acceptable line structures with smooth edges. Materials with high cohesion and film strength, such as certain commercial high-molecular mass light-emitting polymers (LEPs), tend to overwhelm the tearing forces at the line edge, leading to poor image quality. Therefore, industrial applications are rather focused to the patterning of vapor-deposited conventional small molecular phosphorescent emitting materials with less intermolecular forces, which have high electroluminescent efficiencies and long OLED device lifetimes. However, carefully tailored formulation of such polymeric materials as blends with electrically inert host polymers and further hole-transporting materials allowed the deposition of satisfactory line patterns with promising emission characteristics [162, 163]. Receptor substrates are typically glass coated with ITO as the transparent electrode layer and a hole-conducting layer (80 nm thick PEDOT:PSS) spin coated on top of it. In order to improve the adhesion of the transfer layer to the PEDOT-coated receiver, an additional thin siloxane layer was added in order to cover the hydrophilic surface with a hydrophobic ultrathin film to enhance the compatibility and wettability at the interface with the transferred hydrophobic polymer blend [164]. About 80 μm wide stripes of the LEP blend were transferred from donor films precoated with red-, green-, and blue-emitting materials to fabricate OLEDs. In 2003, Samsung SDI presented the first full-color active-matrix OLED display prototypes fabricated with an LITI process step [162]. From Samsung's extensive patent application activities concerning development and refining of technical process equipment compounds during the past years, it might be concluded that the LITI process is already close to industrial integration in full-color OLED flat-panel production lines.

5.4.3.3.5 **Metal Nanoparticle Absorbers**

The size-dependent quantum dot absorbance of colloid Ag NPs has been exploited to build tailored absorptive LTHC layers with an absorption in the visible range [64]. About 100–200 nm thick films of 30–40 nm sized Ag NPs show a strong absorption around 530 nm, which fits the emission of the 532 nm emission of frequency-doubled Nd:YAG lasers. In order to prevent the Ag NPs from aggregation and coalescence into a bulk film during spin coating, they were protected by a self-assembled alkanethiol monolayer (SAM). The absorbing nanomaterial layer is only loosely connected and can therefore be easily vaporized by the laser. The green-emitting OLED material tris-(8-hacroxyquinoline) aluminum (Alq_3) was deposited by an RIR-PLD technique to form 200–300 nm thick layers. The receptor substrate was coated with a siloxane layer as adhesion promoter and placed with a small transfer gap (<100 μm). Pattern transfer of Alq_3 pixels (0.9 mm × 0.9 mm) was obtained in a fluence range of 50–150 mJ cm^{-2}. As an indicator of the conservation of the materials properties the fluorescence of Alq_3 was measured before and after transfer, and the spectra showed no significant alterations. The method has been named *nanomaterial-enabled laser transfer* (NELT). However, it is

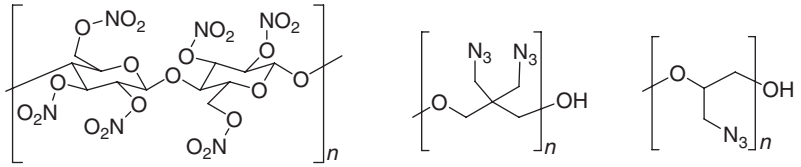

Figure 5.4.7 Chemical structures of nitrogen-rich polymers: nitrocellulose (1), poly-BAMO (2), and glycidyl azide polymer GAP (3).

not clear which amount of the ablated Ag nanoparticle release layer is co-deposited with the molecular OLED material.

5.4.3.3.6 **Absorbing Polymer Release Layer Systems**

The laser-triggered decomposition of energetic gas-generating polymer release layers has been presented in the section on LAT with metal absorbing layers, as well as composites of thermodecomposable polymers doped with black carbon or dispersed IR dyes as radiation absorber. Similarly, LIFT transfer of polymer composites doped with a CNT content of 5–10% (wt), which provides sufficient absorption to interact with a UV laser, has been mentioned above. Chemical structures of some representative nitrogen-rich polymers are shown in Figure 5.4.7. Nitrocellulose (or cellulose nitrate) is a self-oxidizing polymer and its energetic performance depends on the nitrogen content. With a nitrogen content higher than 13% it has been used as ''gun cotton'' and rocket propellant. Poly-BAMO (2) and GAP (3) are energetic polymers with a polyether backbone that bears per repeating unit two, and one azide (N_3) groups, respectively, in the side chains, that can each split off one molecule of elemental nitrogen (N_2) on thermal ignition or appropriate UV irradiation. Immediate decomposition of the labile nitrogen moieties leads to a significant volume expansion by violent gas generation that can be used as a propellant thrust.

Both nitrite ester as well as azide moieties attached as side chains to the polymer main chain show an absorption in the UV range between ~300 and 250 nm. They can therefore be electronically excited by UV light within that range, and a phototriggered decomposition of the nitrogen-containing functional groups can be initiated on irradiation. In another type of tailor-made nitrogen-containing polymers, UV-photocleavable aryltriazene chromophores (Ar–N=N–N–) are covalently incorporated within the polymer backbone [165]. By that, UV laser irradiation of the polymer induces a photofragmentation reaction, and the main chain is cleaved into nitrogen gas and small volatile organic fragments, as outlined in Figure 5.4.8.

Films of such aryltriazene polymers show a high absorption in the range of about 250–350 nm with an absorption coefficient (at 308 nm $\alpha_{lin} \sim 100\,000\ cm^{-1}$) and can be efficiently decomposed on UV exposure [166]. Therefore, films of these photosensitive polymers proved to be excellently suitable for laser ablation applications. The laser fluence threshold for ablation is very low (~20 mJ cm^{-2}), the ablation rates per laser pulse are quite high, the ablated surface patterns are sharp

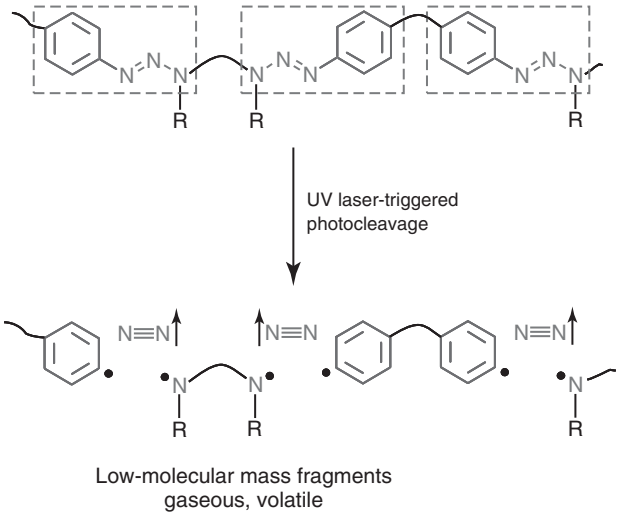

Figure 5.4.8 Schematic general structure of the UV-cleavable polymers. The polymer main chain contains aryl triazene chromophore units (dashed frames), which decompose on UV light irradiation, leading to an irreversible fragmentation of the polymer backbone into small volatile organic fragments and nitrogen gas.

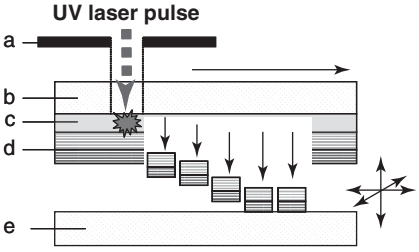

Figure 5.4.9 Principle of the modified laser-induced forward transfer (LIFT) process with an absorbing sacrificial polymer film: (a) mask, (b) carrier substrate, (c) sacrificial thin film of "exploding" aryltriazene photopolymer serving as a pressure generator on laser irradiation, (d) thin layers of transfer material, and (e) receiver substrate with transferred pixels.

and clean, and no debris by redeposition of ablated material or carbonization was observed [73, 167, 168]. The laser-triggered photofragmentation process results in an abrupt volume expansion jet of "ablation" products and a transient high-pressure jump. This effect can be utilized for LIFT applications, when the aryltriazene polymer films are used as absorbing sacrificial DRLs. The overlying film of solid and pure transfer materials is punched out and catapulted integrally toward the receiver surface as outlined in Figure 5.4.9. Various transfer materials were investigated as model systems (e.g., pyrene-doped polymethyl methacrylate (PMMA) films) [169] to define the best process conditions, such as optimum film thickness for the individual material layers with relation to the applied laser fluence [170]. As

examples, the transfer of well-defined pixels of thin polymer films was demonstrated with aqueous-based films of the biopolymer gelatin and a methylated cellulose derivative [170]. The accurate LIFT deposition of thin polymer films has recently been demonstrated for microsensor applications. Homogeneous and hole-free polyethyleneimine (PEI) pixels with a low surface roughness were deposited in the same way with a triazene photopolymer DRL after process optimization [171]. Meanwhile, LIFT of PEI thin films to sensing chip units allowed measuring of chemoresponsive signals [165].

Use of the polymeric DRL also enables the accurate LIFT deposition of metal films. Transferred 80 nm thin aluminum film pixels (500 μm × 500 μm) showed clear-cut edges and a homogeneous layer morphology without traces of splashing or codeposited debris outside the pixel area. It has been found that the mechanical as well as the thermophysical material properties of the transfer layer and carrier substrate have significant effects on the transfer results. Owing to the influence of the thermal diffusion toward the carrier substrate during nanosecond laser pulse duration, the fluence threshold for ablation was found to increase substantially for ultrathin films (<50 nm), depending on the material properties of the carrier material [172].

The spatial shape of the focused laser spot directly defines the outline of the catapulted pixel. Since the sacrificial polymer release layer protects the transfer layer from the incident UV irradiation, even highly sensitive materials can be gently transferred and deposited. Only small and volatile organic fragments are formed by the laser-triggered photopolymer decomposition, and therefore only a minimum of contamination of the transferred deposits may be expected. This is a substantial advantage compared to metal absorbing layers, which are known to be codeposited with the transferred material after laser-induced volatilization during the LIFT process [147]. Compared with previous LTHC layers frequently used with IR lasers, the UV-light-triggered photodecomposition process reduces significantly the heat load to the transfer layer, which is detrimental to the properties or functionality of sensitive materials.

The aryltriazene photopolymers, used as the catapulting layer, were tailored to have an absorption peak that fits the XeCl excimer laser wavelength at 308 nm [173]. The flatter beam energy profile of the less coherent excimer laser is its principal advantage over Gaussian solid-state UV lasers, as this results in a much cleaner transfer. Other lasers that have shown how differences in pulse duration and the beam energy profile affected the quality of the transferred material have been studied [174]. Despite improving the catapulting efficiency, there was no clear advantage of shorter pulse lengths over the standard 30 ns pulse length of the XeCl laser.

The potential of aryltriazene photopolymers as catapulting sacrificial layers in LIFT applications was demonstrated with various highly sensitive materials: assisted by a ~100 nm thick sacrificial triazene polymer, DRL living mammalian neuroblast cells were transferred and gently deposited on a receiver substrate using a 193 nm ArF nanosecond excimer laser [175]. With focused laser spots of about 20 μm in diameter, plaques of cell bundles embedded in an extracellular

matrix were punched out from a donor substrate and transferred to a bioreceiver over a gap of 150 μm above the threshold fluence for cell transfer of 50 mJ cm^{-2}, gentle enough that the functionality was not impaired at all, and the cells started reproducing instantly. After 48 h of the transfer, the cells showed intact preservation of nuclei with well-developed axonal extensions, demonstrating that the technique is competent in creating patterns of viable cells at low fluences. This opens up new possibilities for the manufacture of biosensors in which living cells should be precisely deposited onto microchips. By developing more automated computer-controlled LIFT setups with *in situ* monitoring by charged-coupled detector (CCD) cameras more complex cell arrays can be deposited in a reproducible way, as recently reported [176].

In the same way, semiconducting multispectral nanocrystal quantum dots (NCQDs) were successfully transferred by the photopolymer-assisted LIFT setup into laterally patterned arrays [177]. A patterned metal mask was used for the LIFT deposition of two different sizes of CdSe(CdS) nanoquantum dots (5 and 6 nm in diameter which show yellow and red color) coated on a bilayer of triazene photopolymer DRL and a thin aluminum film as conducting electrode. Interdigitating 6 × 6 matrix arrays with pixel sizes of 800 μm were printed onto ITO-coated glass substrates. PL of the NCQDs before and after transfer was found to be nearly unchanged, indicating the conservation of materials functionality during the transfer.

To prove the validity of the photopolymer-based LIFT approach, a working miniaturized model OLED device has been fabricated [178]. For that, micropixel stacks consisting of a bilayer of the electroluminescent polyparaphenylene vinylene derivative MEH-PPV (poly[2-methoxy-5-(2′-ethylhexyloxy)-p-phenylene vinylene]), together with an aluminum cathode, was transferred onto a receiver substrate coated with a prestructured ITO anode (as shows in Figure 5.4.10). On the fused silica donor carrier three individual thin layers had to be deposited one after

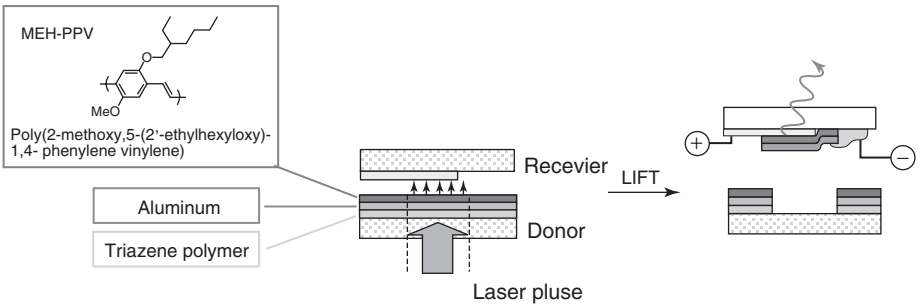

Figure 5.4.10 Layer architecture of the donor and receiver substrate for the pixel transfer with a thin layer (40–90 nm) of the electroluminescent polymer MEH-PPV, the aluminum cathode (70 nm), and the aryltriazene photopolymer film (100 nm). The incident laser pulse decomposes the sacrificial photopolymer layer and catapults the Al/MEH-PPV bilayer system in one step toward the prestructured transparent indium–tin oxide (ITO) anode on top of the receiver surface.

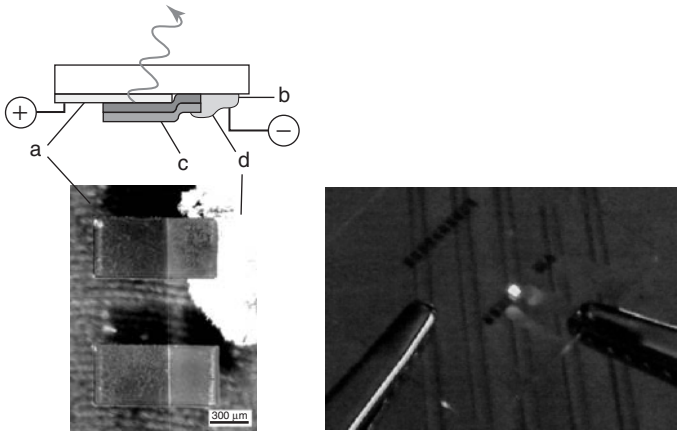

Figure 5.4.11 Resulting OLED pixel device after LIFT: the MEH-PPV layer (b) and cathode (c) are printed onto the ITO anode (a). The photograph shows two adjacent pixels seen through the ITO-coated substrate. After contacting with silver paste (d) the pixel shows an orange–red light emission.

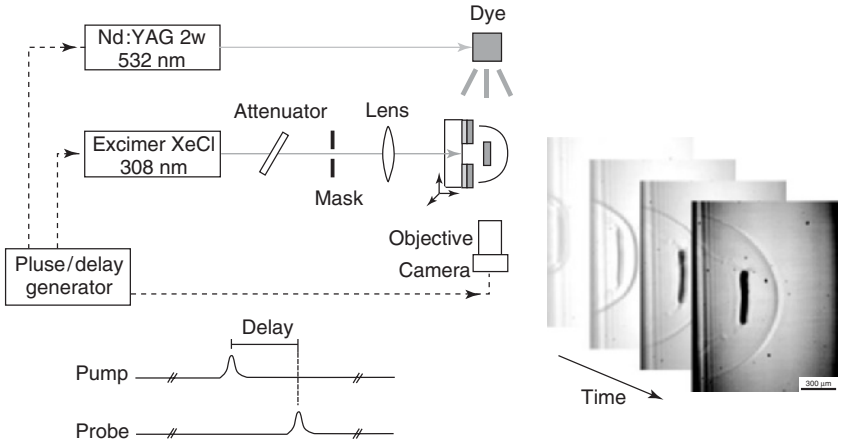

Figure 5.4.12 Setup for the two laser ''pump-probe'' shadowgraphy experiments for time-resolved imaging of the forward transfer processes.

another, corresponding to the inverse stack of the later OLED device: a spin-coated basic triazene photopolymer layer (100 nm) followed by a thermally evaporated Al layer (70 nm), and as the top layer, a spin-coated MEH-PPV film (90 nm) (shown in Figure 5.4.10).

With single nanosecond pulses of a 308 nm XeCl excimer laser, MEH-PPV and the aluminum cathode were directly printed onto the ITO anode in one step. The transferred pixel required that contact be made only with a DC voltage for the emission of orange light (Figure 5.4.11). The functionality of operating devices was characterized by current–voltage and electroluminescence measurements, which

prove that the integrity of the transferred materials has been fully preserved during the improved LIFT deposition process. The transfer process has been further extended, by shaping the laser beam using an appropriate mask, so that a pattern of multiple pixels may be deposited with a single pulse, providing a promising method for the production of full-colored displays on flexible substrates.

To get more insight into the dynamic mechanism of the LIFT process, a time-resolved pump-probe microimaging technique known as *shadowgraphy* was adapted to visualize the ejection of micropixels and the transfer process that also involves the occurrence of shockwaves [179]. The experimental setup for such investigations is outlined in Figure 5.4.12.

Such shockwaves are generated by laser–material interactions, in this case by the laser-triggered ''microexplosion'' of the catapulting layer, and their strengths depend on the pressure of the ambient atmosphere. As an example, the shadowgraphy images in Figure 5.4.13 show the ejection process of a model pixel flyer (80 nm thick film of aluminum on top of 350 nm of absorber polymer) in ambient atmosphere, where the evolving shockwave together with the catapulted pixel can be clearly seen. The upper row of images shows the time-resolved development of the shockwave and the flyer at a constant fluence of 360 mJ cm^{-2} with increasing time intervals (200 ns steps) after the LIFT pump pulse. A bilayer system of 80 nm aluminum on top of a triazene DRL of 350 nm was irradiated at 308 nm with 360 mJ cm^{-2} per pulse. After 200 ns the evolving shockwave together with the ejected flyer appears with a piston-type flat surface. At 400 ns the shockwave appears more hemispherical and propagates with a higher speed than the flyer. The shape and morphology of the catapulted pixel stays intact over a distance of more than 300 μm, as these images show. The second row shows the influence of the applied fluence after a fixed time delay of 800 ns each: the propagation velocity of both the shockwave and the pixel flyer depends on the energy of the incident laser pulse, which allows a fine tuning of the transfer conditions at low fluences. However, at a fluence of already around 1 J cm^{-2} the blast power is high enough to accelerate the flyer more than the shockwave, so that it gets destroyed on interaction. Such time-resolved mechanistic investigations are helpful to define optimized conditions for the LIFT process of various transfer material layer systems. From such shadowgraphy image series, the individual propagation speed of the shockwave and the flyer can be derived depending on the laser fluence and the thickness of the sacrificial DRL. The analysis of these values allowed for deriving the first simple model for the energy balance in order to estimate the conversion efficiency of the incident laser into the kinetic energy of the ejected flyer [180].

For example, solid ceramic thin films of gadolinium gallium oxide and ytterbium-doped yttrium aluminum oxide have been deposited by the sacrificial polymer-assisted LIFT [181]. The dependence of the ablation dynamics and quality of the ejected donor material on the laser fluence and thickness of the sacrificial and donor layers were investigated by means of this shadowgraphy technique. From detailed analyses of such studies, dynamic process parameters and information on the energy conversion can be derived, such as propagation velocities of catapulted flyers and correlated shockwaves that have to be carefully tuned for

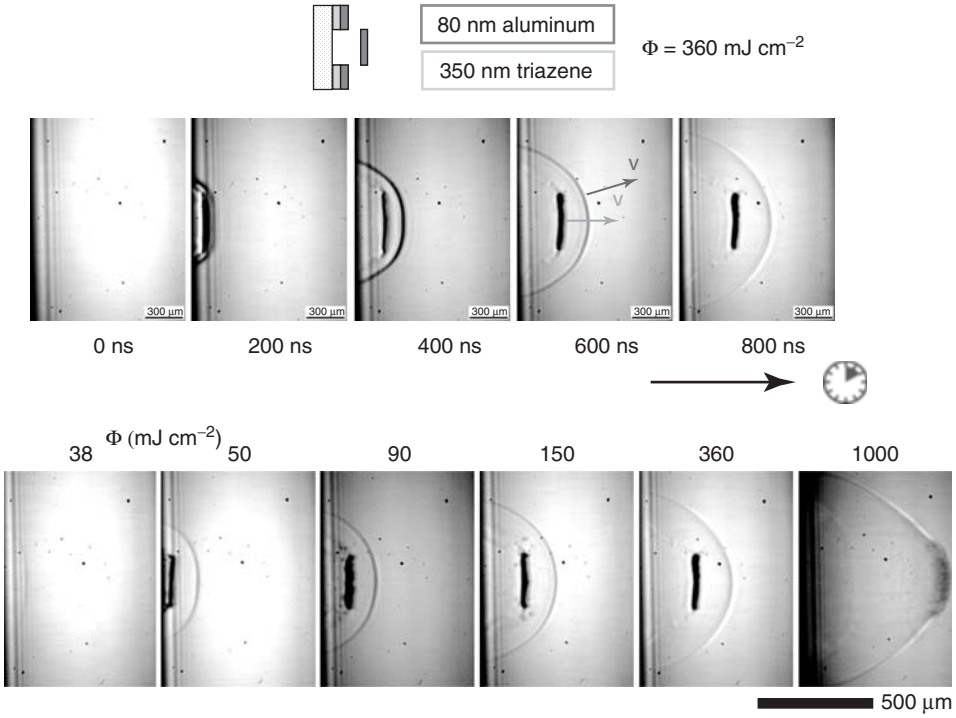

Figure 5.4.13 Shadowgraphy microimages of the time-resolved development of the shockwave and flyer ejection for a laser fluence Φ of 360mJ cm^{-2} (upper row). The flyer consists of a layer of 80 nm aluminum, which was coated on top of a 350 nm thick triazene photopolymer. The flyer stays stable over quite a long distance of more than 0.3 mm. The image sequence shows the different propagation speeds v of the flyer and the shockwave. Second row: The forward ejection of the same model system was studied to investigate the fluence dependence of the generated thrust. Images are taken each at a constant delay time of 800 ns after the laser pulse. Flyer velocity and shockwave shape depend on the applied laser fluence.

successful high-quality LIFT results necessary for reliable device fabrication [180]. Shadowgraphy studies revealed also that a smooth deposition of micropixels over a narrow transfer gap can be crucially disturbed by the interaction of the catapulted flyer with reflected shockwaves [182]. An example of the interaction of the reflected shockwave echo with a thin metal film flyer within a transfer gap of 500 µm is shown in Figure 5.4.14. The evolving shockwave front reaches the receiver substrate after 400 ns and starts to be reflected. As a consequence, the catapulted flyer collides with the shockwave echo. This interaction reduces the speed of the flyer and causes its disintegration before being deposited onto the receiver. Here, proper choice of the pressure conditions and gap distance are further variables in the multiparameter space of the LIFT process.

The functionality of triazene photopolymers as DRL has also been studied with femtosecond laser pulses at 800 nm [183] for the transfer of 10 µm ceramic disc

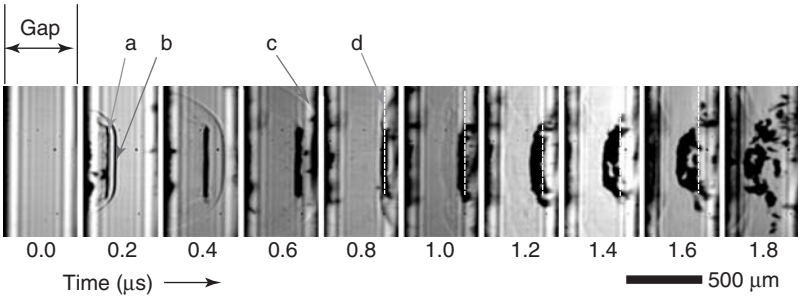

Figure 5.4.14 Shadowgraphy analysis of forward transfer with a gap distance of 0.5 mm. Sequence of images taken with a sample as shown in Figure 5.4.13 (80 nm Al on top of 350 nm triazene polymer DRL) at a fluence of 160 mJ cm^{-2}. After 200 ns time delay, the catapulted flyer (a) and the shockwave front (b) can be seen. When the shockwave has reached the receiver surface, the echo wave starts to be reflected (c), and the velocity of the incoming flyer is slowed down after interaction with the shockwave echo (see the constant position of the flyer front indicated by the dotted line (d) during following 400 ns). Finally, the flyer gets disintegrated into small fragments that are scattered backwards.

pellets [184]. The threshold transfer fluence with the photopolymer DRL was found to be only ~20% of the polymer ablation threshold at the laser wavelength. This behavior is in stark contrast to nanosecond DRL-LIFT using the same polymer, where the transfer threshold is reproducibly found to be slightly greater than the ablation threshold. This decrease has been attributed to ultrafast shockwave generation in the constrained polymer layer under femtosecond irradiation being the driving force for the femtosecond LIFT with the polymer DRL. However, further effects may also play a role here, such as white-light continuum generation in the carrier substrate, as well as standing optical waves [185].

Special Applications Using Femtosecond Lasers The use of femtosecond pulsed lasers has certain advantages, as described above, and can be used for the transfer of very small pixels. Deposition of nanoscale droplets of Cr was achieved using femtosecond Ti:sapphire LIFT, and deposits around 300 nm in diameter are obtained from a 30 nm thick source film [186]. Femtosecond lasers also have the advantage of high repetition rates, and the possibility of beam shaping (temporal and lateral profile). Temporal beam shaping can be used to optimize with feedback loops, while lateral beam shaping can be used to precut (structure) the transfer pixel before transfer. Multiple, subthreshold fluence femtosecond pulses have been used to lessen the adhesion of a donor film to a support substrate to facilitate the subsequent forward transfer step of solid ''pellets.'' To define the area for transfer in ''hard'' solid donor films, such as glasses, crystals, ceramics, and so on, more precisely, and to allow for more reproducible pellet shapes, an outer ring with relatively higher intensity was added to the transfer laser pulses by means of the near-field diffraction pattern of a circular aperture. This approach was called *ballistic laser-assisted solid transfer* (BLAST) [187]. Since BLAST does not require a

DRL material, it is potentially applicable to the forward transfer deposition of any ''hard'' donor. A further laser-based microstructuring technique for the etching and deposition of solid materials, called *laser-induced solid etching* (LISE), utilizes also the absorption of femtosecond-duration laser pulses in a constrained metal film between two bulk substrates [188]. At least one of the two substrates has to be transparent to the laser wavelength. The very rapid pressure increase in the ''sandwiched'' metal film following irradiation is believed to initiate crack propagation in one or the other of the bulk substrates. By spatially shaping the laser beam, the cracking process can be controlled to etch small solid flakes of material from the substrates, and smooth, micron-scale pits and trenches in silicon and silica could be etched using LISE. As a unique feature of LISE, the material etched from the bulk substrate is removed as a single solid piece and is not shattered, melted, or vaporized by the process. Hence, the etched material can be collected on the other bulk substrate used in the process. In this way, micron-scale dots and lines of silica have been deposited onto silicon and vice versa. Minimal evidence of melting during the process has been observed, suggesting that LISE may be a useful technique for the forward transfer direct-write of intact solid materials.

Variation of the DRL LIFT Approach A UV-absorbing poly(ethylene naphthalate) (PEN) foil (1.35 μm, showing the maximum UV–vis absorption λ_{max} around 360 nm) has been applied in a tailored laser-based setup for the contact- and contamination-free collection of histologic material for proteomic and genomic analyses. The sample of interest is prepared by a laser microdissection step followed by laser-induced transport (laser pressure catapulting) toward a collector microvessel [189, 190]. The tissue section is prepared on top of the PEN carrier membrane and the cell transfer achieved with nanosecond pulses of a N_2 laser at 337 nm. Time-resolved ejection dynamics were investigated by an ultrafast imaging system.

5.4.3.3.7 **Blistering Lift-Off Methods**

A 4 μm thick film absorbing layer of polyimide was used for the LIFT deposition of sensitive embryonic stem cells [191]. The film thickness is significantly larger than the laser absorption depth of about 750 nm at the 355 nm laser emission wavelength. In this case, the laser causes vaporization inside the sacrificial layer below the transfer material interface. The polymer expands because of the generated pressure with plastic deformation and builds up a curved blister. The hot gases cool and stay trapped inside the blister cavity, thereby remaining isolated from the transfer material. With appropriate tuning of the laser fluence, viscous materials are ejected from the fast bulging polyimide surface on top of the expanding cavity, and the jetted droplet size increases with increasing laser fluences. At higher laser fluences the polyimide membrane will be more and more ablated and susceptible to rupture. When the film ruptures, hot vapor from the ablation process is able to escape into the transfer material layer and blow it locally away, leading to a more energetic explosive ejection and deposition process that was found to lead to splashes. Transfer of viable mouse embryonic stem cells spread

as a glycerol/cell growth media suspension on the polyimide sacrificial layer was successfully achieved over a 100 μm gap.

Titanium metal coatings with a thickness far above the absorption length at 532 nm emission were used in a setup similar to the blistering membrane [192]. The metal layer was coated with a ~1 μm thick layer of ultradispersed diamond (particle size below 200 nm) and irradiated with single 50 ps pulses. Transfer of the diamond nanopowder over a defined gap was observed between a minimum threshold fluence and the fluence for total ablation of the Ti layer, whereby the deposited diamond nanopowder was accompanied by deposition of metal droplets on the acceptor substrate (ablative transfer). In an intermediate fluence regime between these critical values, the Ti film stays optically intact without perforations and cracks. Ejection of the nanopowder can be attributed to a fast movement of the transient blister at the metal-quartz-carrier interface and the shock waves. With these transfer conditions, the transfer layer stays completely isolated from the incoming radiation and ablation products of the sacrificial layer, but the transfer efficiency is limited by the adhesion of the transfer material to the blistering layer. Since the ejection of the particles starts on top of an expanding membrane-like convexity, a fluence-dependent transverse scattering of the deposited particles was observed. Even when the method of blister-based LIFT seems to be limited to powders or viscous suspensions, it offers an interesting potential for the transfer of wet biomaterials that can be used for biodevice fabrication with complete shielding of the laser radiation.

5.4.3.3.8 **Other Methods**

With a polyimide-absorbing sacrificial polymer release layer, a method was reported for the laser-driven release on demand of prefabricated microstructures [193]. This DRL-LIFT-based approach was used for the batch assembly of hybrid microelectromechanical systems (MEMS) built from parts fabricated on different substrates. A classic photolithographic process has been applied to build up about 100 μm high microstructured components, but on top of a polyimide basis layer that is later used as the absorbing DRL. For the assembly step, prefabricated parts are aligned and fitted together by LIFT catapulting of the prepared microstructure to the chip with a KrF excimer laser. The same procedure was adapted later for the LIFT deposition of more complex bar die device units and Si substrates, including commercial LM555 timer chips [194]. As a proof of principle, a blinker circuit was assembled by laser transferring each of its submillimeter-sized components to a common chip board. An excimer laser was preferentially used with respect to its larger area beam capable of uniformly irradiating a bigger surface of the device, allowing for the transfer to occur with a single laser pulse. The release and transfer of single unpackaged semiconductor devices into a pocket or recess in a substrate enables the LIFT technique to perform the same way as pick-and-place machines used in circuit board assembly to fabricate embedded microelectronic circuits. As a demonstration example, a 300 μm × 300 μm sized InGaN LED was laser deposited and it emitted light when powered [195].

5.4.4
Conclusions and Future Aspects

LIFT has matured since the early reports in the early 1970s and 1986 from a curiosity to a process with many variations, as exemplified by the large number of acronyms (LAT, LITI, LILT, MAPLE-DW, AFA-LIFT, BLAST, LISE, etc.) for the process. The range of transferred materials has also steadily increased from single inorganic compounds such as metals, to imaging dyes and inks, and further to functionally defined multilayers and highly complex and sensitive biological systems. Optimization of the process for individual materials and applications by more insight in the involved mechanisms of the dynamic processes have finally led to LIFT being applied for the fabrication of working devices, such as miniaturized OLEDs or chemosensors. In summary, the recent developments suggest that variations of the LIFT technology rather than the LITI process will be used as industrial fabrication methods.

Acknowledgments

The authors acknowledge the Swiss National Science Foundation (SNSF), the Paul Scherrer Institut (PSI), and Swiss Federal Laboratories for Materials Science and Technology (EMPA) for financial support of their research presented herein. A part of their present work has been financially supported by the FP 7 European project e-LIFT(project n° 247868 –call FP7-ICT-2009-4).

References

1. Kyrkis, K.D., Andreadaki, A.A., Papazoglou, D.G., and Zergioti, I. (2006) in *Recent Advances in Laser Processing of Materials* (eds J. Perrière, E. Millon, and E. Fogarassy), Elsevier, pp. 213–241.
2. Arnold, C.B., Serra, P., and Piqué, A. (2007) Laser direct-write techniques for printing of complex materials. *MRS Bull.*, **32**, 23–31.
3. Madou, M.J. (1997) *Fundamentals of Microfabrication*, CRC Press LLC.
4. Quist, A.P., Pavlovic, E., and Oscarsson, S. (2005) Recent advances in microcontact printing. *Anal. Bioanal. Chem.*, **381**, 591–600.
5. Wilbur, J.L., Kumar, A., Biebuyck, H.A., Kim, E., and Whitesides, G.M. (1996) Microcontact printing of self-assembled monolayers: applications in microfabrication. *Nanotechnology*, **7**, 452.
6. Blanchet, G. and Rogers, J. (2003) Printing techniques for plastic electronics. *J. Imaging Sci. Technol.*, **47**(4), 296–303.
7. Hobby, A. (1990) Fundamentals of screens for electronics screen printing. *Circuit World*, **16**(4), 16–28.
8. Carr, B.P. (1994) Introduction to thick film fine line printing screens. *Microelectron. Int.*, **11**(1), 4–7.
9. Pardo, D.A., Jabbour, G.E., and Peyghambarian, N. (2000) Application of screen printing in the fabrication of organic light-emitting devices. *Adv. Mater.*, **12**(17), 1249–1252.
10. Calvert, P. (2001) Inkjet printing for materials and devices. *Chem. Mater.*, **13**(10), 3299–3305.
11. de Gans, B.-J., and Schubert, U.S. (2004) Inkjet printing of well-defined polymer dots and arrays. *Langmuir*, **20**(18), 7789–7793.

12. Gamerith, S., Klug, A., Scheiber, H., Scherf, U., Moderegger, E., and List, E.J.W. (2007) Direct ink-jet printing of Ag-Cu nanoparticle and Ag-precursor based electrodes for OFET applications. *Adv. Funct. Mater.*, **17**(16), 3111–3118.
13. Ko, S.H., Chung, J., Pan, H., Grigoropoulos, C.P., and Poulikakos, D. (2007) Fabrication of multilayer passive and active electric components on polymer using inkjet printing and low temperature laser processing. *Sens. Actuator A*, **134**(1), 161–168.
14. Plötner, M., Wegener, T., Richter, S., Howitz, S., and Fischer, W.-J. (2004) Investigation of ink-jet printing of poly-3-octylthiophene for organic field-effect transistors from different solutions. *Synth. Met.*, **147**(1–3), 299–303.
15. Lewis, J.A. and Gratson, G.M. (2004) Direct writing in three dimensions. *Mater. Today*, (July/August) 32–39.
16. Therriault, D., White, S.R., and Lewus, J.A. (2003) Chaotic mixing in three-dimensional microvascular networks fabricated by direct-write assembly. *Nat. Mater.*, **2**, 265–271.
17. Eason, R.W. (2007) *Pulsed Laser Deposition of Thin Films Applications-Led Growth of Functional Materials*, John Wiley & Sons, Inc., Hoboken, NJ.
18. Chrisey, D.B. and Hubler, G.K. (1994) *Pulsed Laser Deposition of Thin Films*, John Wiley & Sons, Inc., New York.
19. Blanchet, G.B. (1995) Deposition of poly(methyl methacrylate) films by UV laser ablation. *Macromolecules*, **28**, 4603–4607.
20. Blanchet, G.B. (1996) Prepare fluoropolymer films using laser ablation. *Chemtech*, **26**(6), 31–35.
21. Chrisey, D.B., Pique, A., McGill, R.A., Horwitz, J.S., Ringeisen, B.R., Bubb, D.M., and Wu, P.K. (2003) Laser deposition of polymer and biomaterial films. *Chem. Rev.*, **103**, 553–576.
22. Yang, X., Tang, Y., Yu, M., and Qin, Q. (2000) Pulsed laser deposition of aluminum tris-8-hydroxyquinline thin films. *Thin Solid Films*, **358**(1–2), 187–190.
23. Chrisey, D.B., Pique, A., Fitz-Gerald, J., Auyeung, R.C.Y., McGill, R.A., Wu, H.D., and Duignan, M. (2000) New approach to laser direct writing active and passive mesoscopic circuit elements. *Appl. Surf. Sci.*, **154**, 593–600.
24. Losekrug, B., Meschede, A., and Krebs, H.U. (2007) Pulsed laser deposition of smooth poly(methyl methacrylate) films at 248 nm. *Appl. Surf. Sci.*, **254**(4), 1312–1315.
25. Suske, E., Scharf, T., Krebs, H.U., Junkers, T., Buback, M., Suske, E., Scharf, T., Krebs, H.U., Junkers, T., and Buback, M. (2006) Mechanism of poly(methyl methacrylate) film formation by pulsed laser deposition. *J. Appl. Phys.*, **100**(1), 014906.
26. Kecskemeti, G., Smausz, T., Kresz, N., Toth, Zs., Hopp, B., Chrisey, D., and Berkesi, O. (2006) Pulsed laser deposition of polyhydroxybutyrate biodegradable polymer thin films using ArF excimer laser. *Appl. Surf. Sci.*, **253**, 1185–1189.
27. Blanchet, G.B. and Fincher, C.R. (1994) Laser-induced unzipping–a thermal route to polymer ablation. *Appl. Phys. Lett.*, **65**(10), 1311–1313.
28. Blanchet, G.B. and Fincher, C.R. (1994) Thin-film fabrication by laser-ablation of addition polymers. *Adv. Mater.*, **6**(11), 881–887.
29. Purice, A., Schou, J., Kingshott, P., Pryds, N., and Dinecu, M. (2007) Characterization of lysozyme films produced by matrix assisted pulsed laser evaporation (MAPLE). *Appl. Surf. Sci.*, **253**, 6451–6455.
30. Bubb, D.M., Toftman, B., Haglund, R.F. Jr., Horwitz, J.S., Papantonakis, M.R., McGill, R.A., Wu, P.W., and Chrisey, D.B. (2002) Resonant infrared pulsed laser deposition of thin biodegradable polymer films. *Appl. Phys. A*, **74**, 123–125.
31. Toftmann, B., Papantonakis, M.R., Auyeung, R.C.Y., Kim, W., O'Malley, S.M., Bubb, D.M., Horwitz, J.S., Schou, J., Johansen, P.M., and Haglund, R.F. Jr. (2004) UV and RIR matrix assisted pulsed laser deposition of organic MEH-PPV films. *Thin Solid Films*, **453–454**, 177–181.
32. Lantz, K.R., Pate, R., Stiff-Roberts, A.D., Duffell, A.G., and Smith, E.R.

(2009) Comparison of conjugated polymer deposition techniques by photoluminescence spectroscopy. *J. Vac. Sci. Technol. B*, **27**(5), 2227–2231.
33. Johnson, S.L., Park, H.K., and Haglund, R.F. Jr. (2007) Properties of conductive polymer films deposited by infrared laser ablation. *Appl. Surf. Sci.*, **253**, 6430–6434.
34. Braudy, R.S. (1969) Laser writing. *Proc. IEEE*, **57**, 1771–1772.
35. Levene, M.L., Scott, R.D., and Siryj, B.W. (1970) Material transfer recording. *Appl. Opt.*, **9**(10), 2260–2265.
36. Roberts, D.L. (1971) Laser Recording technique using combustible blow-off. US Patent 3, 787, 210, The National cash Register Comp., Dayton, filed Sept. 30, 1971.
37. Peterson, J.O.H. (1974) Printing plate by laser transfer. US Patent 3, 964, 398, Scott Paper Comp., Philadelphia, filed Jan. 17, 1974.
38. Bohandy, J., Kim, B., and Adrian, F.J. (1986) Metal deposition from a supported metal film using an excimer laser. *J. Appl. Phys.*, **60**(4), 1538–1539.
39. Veiko, V.P., Shakhno, E.A., Smirnov, V.N., Mioskovski, A.M., and Nikishin, G.D. (2006) Laser-induced film deposition by LIFT: physical mechanisms and applications. *Laser Part. Beams*, **24**, 203–209.
40. Claeyssens, F., Klini, A., Mourka, A., and Fotakis, C. (2007) Laser patterning of Zn for ZnO nanostructure growth: comparison between laser induced forward transfer in air and in vacuum. *Thin Solid Films*, **515**, 8529–8533.
41. Baum, H.H. and Comita, P.B. (1992) Laser-induced chemical vapor deposition of metals for microelectronics technology. *Thin Solid Films*, **218**, 80–94.
42. Grenon, B.J. *et al.* (1997) Methods for repair of photomasks. US Patent 6, 165, 649, IBM Corporation, Inv., filed Jan. 21, 1997.
43. Germain, C., Charron, L., Lilge, L., and Tsui, Y.Y. (2007) Electrodes for microfluidic devices produced by laser-induced forward transfer. *Appl. Surf. Sci.*, **253**, 8328–8333.
44. Chrisey, D.B., Pique, A., Fitz-Gerald, J., Auyeung, R.C.Y., McGill, R.A., Wu, H.D., and Duignan, M. (2000) New approach to laser direct writing active and passive mesoscopic circuit elements. *Appl. Surf. Sci.*, **154–155**, 593–600.
45. Zergioti, I., Mailis, S., Vainos, N.A., Papakonstantinou, P., Kalpouzos, C., Grigoropoulos, C.P., and Fotakis, C. (1998) Microdeposition of metal and oxide structures using ultrashort laser pulses. *Appl. Phys. A*, **66**, 579–582.
46. Zergioti, I., Mailis, S., Vainos, N.A., Fotakis, C., Chen, S., and Grigropoulos, C.P. (1998) Microdeposition of metals by femtosecond excimer laser. *Appl. Surf. Sci.*, **127–129**, 601–605.
47. Papakonstantinou, P., Vainos, N.A., and Fotakis, C. (1999) Microfabrication by UV femtosecond laser ablation of Pt, Cr and indium oxide thin films. *Appl. Surf. Sci.*, **151**, 159–170.
48. Klini, A., Loukakos, P.A., Gra, D., Manousaki, A., and Fotakis, C. (2008) Laser induced forward transfer of metals by temporally shaped femtosecond laser pulses. *Opt. Express*, **16**(15), 11300–11309.
49. Shah, A., Parashar, A., Singh Mann, J., and Sivakumar, N. (2009) Interference assisted laser induced forward transfer for structured patterning. *Open Appl. Phys. J.*, **2**, 49–52.
50. Landström, L., Klimstein, J., Schrems, G., Piglmayer, K., and Bäuerle, D. (2004) Single-step patterning and the fabrication of contact masks by laser-induced forward transfer. *Appl. Phys. A*, **78**, 537–538.
51. Othon, C.M., Laracuente, A., Ladouceur, H.D., and Ringeisen, B.R. (2008) Sub-micron parallel laser direct-write. *Appl. Surf. Sci.*, **255**, 3407–3413.
52. Narazaki, A., Sato, T., Kurosaki, R., Kawaguchi, Y., and Niino, H. (2008) Nano- and microdot array formation of FeSi_2 by nanosecond excimer laser-induced forward transfer. *Appl. Phys. Express*, **1**, 057001-1–057001-3.
53. Willis, D.A. and Grosu, V. (2005) Microdroplet deposition by laser-induced

forward transfer. *Appl. Phys. Lett.*, **86**, 244103.

54. Lee, B.-G. (2009) Improvement of conductive micropattern in a LIFT process with a polymer coating layer. *Electron. Mater. Lett.*, **5**(1), 29–33.
55. Chen, K.T., Lin, Y.H., Ho, J.-R., Cheng, J.-W.J., Liu, S.-H., Liao, J.-L., and Yan, J.-Y. (2010) Laser-induced implantation of silver particles into poly(vinyl alcohol) films and its application to electronic-circuit fabrication on ecapsulated organic electronics. *Microelectron. Eng.*, **87**, 543–547.
56. Rigout, M.L.A., Niu, H., Qin, C., Zhang, L., Li, C., Bai, X., and Fan, N. (1998) Fabrication and photoluminescence of hyperbranched silicon nanowire networks on silicon substrates by laser-induced forward transfer. *Nanotechnology*, **19**, 245303 (5pp).
57. Fuller, S.B., Wilhelm, E.J., and Jacobson, J.M. (2002) Ink-jet printed nanoparticle microelectromechanical systems. *J. Microelechtromech. Syst.*, **11**(1), 54–60.
58. Auyeung, R.C.Y., Kim, H., Mathews, S.A., and Piqué, A. (2007) Laser direct-write of metallic nanoparticle inks. *J. Laser Micro/Nanoeng.*, **2**(1), 21–25.
59. Kinzel, E.C., Su, S., Lewis, B.R., Laurendeau, N.M., and Lucht, R.P. (2006) Direct writing ov conventional thick film inks using MAPLE-DW process. *J. Laser Micro/Nanoeng.*, **1**(1), 74–78.
60. Young, D., Auyeung, R.C.Y., Piqué, A., Chrisey, D.B., and Dlott, D.D. (2002) Plume and jetting regimes in a laser based forward transfer process as observed by time-resolved optical microscopy. *Appl. Surf. Sci.*, **197–198**, 181–187.
61. Piqué, A., Auyeung, R.C.Y., Metkus, K.M., Kim, H., Mathews, S., Bailey, T., Chen, X., and Young, L.J. (2008) Laser decal transfer of electronic materials with thin film characteristics. *Proc. SPIE*, **6879**, 687911.
62. Piqué, A., Auyeung, R.C.Y., Kim, H., Metkus, K.M., and Mathews, S.A. (2008) Digital microfabrication by laser decal transfer. *J. Laser Micro/Nanoeng.*, **3**(3), 163–168.
63. Auyeung, R.C.Y., Kim, H., Birnbaum, A.J., Zalalutidinov, M., Mathews, S.A., and Piqué, A. (2009) Laser decal transfer of free-standing microcantilevers and microbridges. *Appl. Phys. A*, **97**, 513–519.
64. Ko, S.H., Pan, H., Ryu, S.G., Misra, N., Grigoropoulos, C.P., and Park, H.K. (2008) Nanomaterial enabled laser transfer for organic light emitting material direct writing. *Appl. Phys. Lett.*, **93**, 151110.
65. Nakata, Y., Okada, T., and Maeda, M. (2002) Transfer of laser dye by laser-induced forward transfer. *Jpn. J. Appl. Phys.*, **41**(7B, 2), L839–L841.
66. Gupta, R.K., Gosh, K., and Kahol, P.K. (2009) Fabrication and electrical characterization of Schottky diode based on 2-amino-4, 5-imidazoledicarbonitrile (AIDCN). *Phys. E*, **41**(10), 1832–1834.
67. Blanchet, G.B., Fincher, C.R., and Malajovich, I. (2003) Laser evaporation and the production of pentacene films. *J. Appl. Phys.*, **94**(9), 6181–6184.
68. Guy, S., Guy, L., Bensalah-Ledoux, A., Pereira, A., Grenard, V., Cossoa, O., and Vauteya, T. (2009) Pure chiral organic thin films with high isotropic optical activity synthesized by UV pulsed laser deposition. *J. Mater. Chem.*, **19**, 7093–7097.
69. Rapp, L., Diallo, A.K.K., Alloncle, A.P., Videlot-ckermann, C., Fages, F., and Delaporte, P. (2009) Pulsed-laser printing of organic thin-film transistors. *Appl. Phys. Lett.*, **95**, 171109-1–171109-3.
70. Chang-Jian, S.-K., Ho, J.-R., Cheng, J.-W.J., and Sung, C.-K. (2006) Fabrication of carbon nanotube field emission cathodes in patterns by a laser transfer method. *Nanotechnology*, **17**, 1184–1187.
71. Boutopoulos, C., Pandis, C., Giannakopoulos, K., Pissis, P., and Zergioti, I. (2010) Polymer/carbon nanotube composite patterns via laser induced forward transfer. *Appl. Phys. Lett.*, **96**, 041104.
72. Srinivasan, R. and Mayne-Banton, V. (1982) Self-developing photoetching of

poly(ethylene terephthalate) films by far-ultraviolet excimer laser radiation. *Appl. Phys. Lett.*, **41**(6), 576–578.

73. Lippert, T. and Dickinson, J.T. (2003) Chemical and spectroscopic aspects of polymer ablation: special features and novel directions. *Chem. Rev.*, **103**, 453–485.

74. Thomas, B., Alloncle, A.P., Delaporte, P., Sentis, M., Sanaur, S., Barret, M., and Collot, P. (2007) Experimental investigations of laser-induced forward transfer process of organic thin films. *Appl. Surf. Sci.*, **254**, 1206–1210.

75. Karaiskou, A., Zergioti, I., Fotakis, C., Kapsetaki, M., and Kafetzoupoulos, D. (2003) Microfabrication of biomaterials by the su-ps laser-induced forward transfer process. *Appl. Surf. Sci.*, **208–209**, 245–249.

76. Zergioti, I., Karaiskou, A., Papazolou, D.G., Fotakis, C., Kapsetaki, M., and Kafetzopoulos, D. (2005) Time-resolved schlieren study of sub-picosecond and nanosecond laser transfer of biomaterials. *Appl. Surf. Sci.*, **247**, 584–589.

77. Tsuboi, Y., Furuhat, Y., and Kitamura, N. (2007) A sensor for adenosine triphosphate fabricated by laser-induced forward transfer of luciferase onto poly(diemthylsiloxane) microchip. *Appl. Surf. Sci.*, **253**, 8422–8427.

78. Lang, F., Leiderer, P., and Georgiou, S. (2004) Phase transition dynamics measurements in superheated liquids by monitoring the ejection of nanometer-thick films. *Appl. Phys. Lett.*, **85**(14), 2759–2761.

79. Lang, F. and Leiderer, P. (2006) Liquid-vapour phase transitions at interfaces: sub-nanosecond investigations by monitoring the ejection of thin liquid films. *New J. Phys.*, **8**, 14 (10 pp).

80. Modi, R., Wu, H.D., Auyeung, R.C.Y., Gilmore, C.M., and Chrisey, D.B. (2001) Direct writing of polymer thick film resistors using a novel laser transfer technique. *J. Mater. Res.*, **16**(11), 3214–3222.

81. Piqué, A., Chrisey, D.B., Auyeung, R.C.Y., Fitz-Gerald, J., Wu, H.D., McGill, R.A., Lakeou, S., Wu, P.K., Nyuyen, V., and Duignan, M. (1999) A novel laser transfer process for direct writing of electronic and sensor materials. *Appl. Phys. A*, **69** (Suppl.), S279–S284.

82. Fitz-Gerald, J.M., Wu, H.D., Piqué, A., Horwitz, J.S., Auyeung, R.C.Y., Chang, W., Kim, W.J., and Chrisey, D.B. (2000) MAPLE Direct Write: a new approach to fabricate ferroelectric thin film devices in air at room temperature. *Integr. Ferroelectr.*, **29**(1–2), 13–28.

83. Piqué, A., Chrisey, D.B., Fitz-Gerald, J.M., McGill, R.A., Auyeung, R.C.Y., Wu, H.D., Kakeou, S., Nyuyen, V., Chung, R., and Duignan, M. (2000) Direct writing of electronic and sensor materials using a laser transfer technique. *J. Mater. Res.*, **15**(9), 1872–1875.

84. Young, D., Wu, H.D., Auyeung, R.C.Y., Modi, R., Fitz-Gerald, J., Piqué, A., and Chrisey, D.B. (2001) Dielectric properties of oxide structures by a laser-based direct-writing method. *J. Mater. Res.*, **16**(6), 1720–1725.

85. Chrisey, D.B., Piqué, A., Modi, R., Wu, H.D., Auyeung, R.C.Y., and Young, H.D. (2000) Direct writing of conformal mesoscopic electronic devices by MAPLE-DW. *Appl. Surf. Sci.*, **168**, 345–352.

86. Zang, C., Liu, D., Mathews, S.A., Graves, J., Schaefer, T.M., Gilbert, B.K., Modi, R., Wu, H.-D., and Chrisey, D.B. (2003) Laser direct-write and ist application in low temperature Co-fired ceramic (LTCC) technology. *Microelectron. Eng.*, **70**, 41–49.

87. Modi, R., Wu, H.D., Auyeung, R.C.Y., Vollmers, J.E.S., and Chrisey, D.B. (2002) Ferroelectric capacitors made by a laser forward transfer technique. *Integr. Ferroelectr.*, **42**, 79–95.

88. Pique, A., Auyeung, R.C.Y., Stepnowiski, J.L., Weir, D.W., Arnold, C.B., McGill, R.A., and Chrisey, D.B. (2003) Laser processing of polymer thin films for chemical sensor applications. *Surf. Coat. Technol.*, **163–164**, 293–299.

89. Arnold, C.B., Kim, H., and Piqué, A. (2004) Laser direct write of planar alkaline microbatteries. *Appl. Phys. A*, **79**, 417–420.

90. Wartena, R., Curtright, A.E., Arnold, C.B., Piqué, A., and Swider-Lyons, K.E. (2004) Li-ion microbatteries generated by a laser direct-write method. *J. Power Sources*, **126**, 193–202.

91. Kim, H., Kushto, G.P., Arnold, C.B., Kafafi, Z.H., and Piqué, A. (2004) Laser processing of nanocrystalline TiO_2 films for dye-sensitized solar cells. *Appl. Phys. Lett.*, **85**, 464.

92. Chrisey, D.B., Piqué, A., Mc Gill, R.A., Horwitz, J.S., Ringeisen, B.R., Bubb, D.M., and Wu, P.K. (2003) Laser deposition of polymer and biomaterial films. *Chem. Rev.*, **103**, 553–576.

93. Wu, P.K., Ringeisen, B.R., Callahan, J., Brooks, M., Bubb, D.M., Wu, H.D., Piqué, A., Spargo, B., Mc Gill, R.A., and Chrisey, D.B. (2001) The deposition, structure, pattern deposition of biomaterial thin films by matrix-assisted pulsed-laser evaporation (MAPLE) and MAPLE direct write. *Thin Solid Films*, **398–399**, 607–614.

94. Ringeisen, B.R., Chrisey, D.B., Piqué, A., Young, H.D., Modi, R., Bucaro, M., Jones-Meehan, J., and Spargo, B.J. (2002) Generation of mesoscopic patterns of viable Escherichia doli by ambient laser transfer. *Biomaterials*, **23**, 161–166.

95. Wu, P.K., Ringeisen, B.R., Krizman, D.B., Frondoza, C.G., Brooks, M., Bubb, D.M., Auyeung, R.C.Y., Piqué, A., Spargo, B., McGill, R.A., and Chrisey, D.B. (2003) Laser transfer of biomaterials: matrix-assisted pulsed laser evaporation (MAPLE) and MAPLE direct write. *Rev. Sci. Instrum.*, **74**(4), 2546–2557.

96. Barron, J.A., Ringeisen, B.R., Kim, H., Spargo, B.J., and Chrisey, D.B. (2004) Application of laser printing to mammalian cells. *Thin Solid Films*, **453–454**, 383–387.

97. Fukumura, H., Kohji, Y., Nagasawa, K., and Masuhara, H. (1994) Laser implantation of pyrene molecules into poly(methyl methacrylate) films. *J. Am. Chem. Soc.*, **116**, 10304–10305.

98. Fukumura, H. (1997) Laser molecular implantation into polymer solids induced by irradiation below ablation threshold. *J. Photochem. Photobiol. A*, **106**, 3–8.

99. Karnakis, D.M., Goto, M., Ichinose, N., Kawanishi, S., and Fukumura, H. (1998) Forward-transfer laser implantation of pyrene molecules in a solid polymer. *Appl. Phys. Lett.*, **73**(10), 1439–1441.

100. Fukumura, H., Uji-i, H., Banjo, H., Masuhara, H., Karnakis, D.M., Ichinose, N., Kawanishi, S., Uchida, K., and Irie, M. (1998) Laser implantation of photochromic molecules into polymer films: a new approach towards molecular device fabrication. *Appl. Surf. Sci.*, **127–129**, 761–766.

101. Karnakis, D.M., Lippert, T., Ichinose, N., Kawanishi, S., and Fukumura, H. (1998) Laser induced molecular transfer using ablation of a triazeno-polymer. *Appl. Surf. Sci.*, **127–129**, 781–786.

102. Asahi, T., Yoshikawa, H.Y., Yashiro, M., and Masuhara, H. (2002) Femtosecond laser ablation transfer and phase transition of phthalocyanine solids. *Appl. Surf. Sci.*, **197–198**, 777–778.

103. Kishimoto, M., Hobley, J., Goto, M., and Fukumura, H. (2001) Microscopic laser patterning of functional organic molecules. *Adv. Mater.*, **13**(15), 1155–1158.

104. Pihosh, Y., Goto, M., Oishi, T., Kasahara, A., and Tosa, M. (2006) Process during laser implantation and ablation of Copumarin 6 in poly(butyl methacrylate) films. *J. Photochem. Photobiol. A*, **183**, 292–296.

105. Foley, D.M., Bennett, E.W., and Slifkin, S.C. (1991) Ablation-transfer imaging/recording. US Patent 5, 156, 938, (Graphics Technology Int.), filed May 29, 1991.

106. Sandy Lee, I.Y., Tolbert, W.A., Dlott, D.D., Doxtader, M.M., Foley, D.M., Arnold, D.R., and Willis, E.W. (1992) Dynamics of laser ablation transfer imaging investigated by ultrafast microscopy. *J. Imaging Sci. Technol.*, **36**(2), 180–187.

107. Seyfang, B.C., Fardel, R., Lippert, T., Scherer, G.G., and Wokaun, A. (2009) Micro-patterning for polymer electrolyte fuel cells: single pulse laser

ablation of aluminium films from glassy carbon. *Appl. Surf. Sci.*, **255**, 5471–5475.

108. Tolbert, W.A., Sandy Lee, I.-Y., Doxtader, M.M., Ellis, E.W., and Dlott, D.D. (1993) High-speed color imaging by laser ablation transfer with a dynamic release layer: Fundamental Mechanisms. *J. Imaging Sci. Technol.*, **37**(4), 411–422.

109. Sandy Lee, I.Y., Wen, X., Tolbert, W.A., Dlott, D.D., Doxtader, M.M., and Arnold, D.R. (1992) Direct measurement of polymer temperature during laser ablation using a molecular thermometer. *J. Appl. Phys.*, **72**(6), 2440–2448.

110. Tolbert, W.A., Sandy Lee, I.Y., Wen, X., and Dlott, D.D. (1993) Laser ablation transfer imaging using picosecond optical pulses: ultra-high speed, lower threshold and high resolution. *J. Imaging Sci. Technol.*, **37**(5), 485–489.

111. Kinoshita, M., Hasihino, K., and Kitamura, T. (2000) Mechanism of dye thermal transfer from ink donor layer to receiving sheet by laser heating. *J. Imaging Sci. Technol.*, **44**(2), 105–110.

112. Bills, R.E., Chou, H.-H., Dower, W.V., and Wolk, M.B. (1993) Laser propulsion transfer using black metal coated substrates. US Patent 5, 308, 737, Minnesota Mining and Manufacturing Comp., filed Mar. 18, 1993.

113. Phipps, C.R., Luke, J.R., McDuff, G.G., and Lippert, T. (2003) Laser-driven micro-rocket. *Appl. Phys. A*, **77**, 193–201.

114. Urech, L., Lippert, T., Phipps, C.R., and Wokaun, A. (2007) Polymers as fuel for laser-based microthrusters: An investigation of thrust, material, plasma and shockwave properties. *Appl. Surf. Sci.*, **253**, 7646–7650.

115. Lippert, T., Urech, L., Fardel, R., Nagel, M., Phipps, C.R., and Wokaun, A. (2008) Materials for laser propulsion: ''liquid'' polymers. *Proc. SPIE*, **7005**, 700512.

116. Irie, M. and Kitamura, T. (1993) High-definition thermal transfer printing using laser heating. *J. Imaging Sci. Technol.*, **37**(3), 231–235.

117. Irie, M., Kato, M., and Kitamura, T. (1993) Thermal transfer color printing using laser heating. *J. Imaging Sci. Technol.*, **37**(3), 235–238.

118. Irie, M. (2003) 1.0 W high–power small-sized Nd: Yttrium Aluminium Garnet (YAG) laser optical Head for a laser-induced printing system. *Jpn. J. Appl. Phys.*, **42** (Part I, 4A), 1633–1636.

119. Sameshima, T. (1996) Laser beam application to thin film transistors. *Appl. Surf. Sci.*, **96–98**, 352–358.

120. Toet, D., Thompson, M.O., Smith, P.M., and Sigmon, T.W. (1999) Laser assisted transfer of silicon by explosive hydrogen release. *Appl. Phys. Lett.*, **74**(15), 2170–2172.

121. Toet, D., Smith, P.M., Sigmon, T.W., and Thompson, M.O. (2000) Spatially selective materials deposition by hydrogen-assisted laser-induced transfer. *Appl. Phys. Lett.*, **77**(2), 307–309.

122. Toet, D., Smith, P.M., Sigmon, T.W., and Thompson, M.O. (2000) Experimental and numerical investigations of hydrogen-assisted laser-induced materials transfer procedure. *J. Appl. Phys.*, **87**(7), 3537–3546.

123. Lin, Z., Zhigilei, L.V., and Celli, V. (2008) Electron-phonon coupling and electron heat capacity of metals under conditions of strong electron-phonon nonequilibrium. *Phys. Rev. B*, **77**, 075133.

124. Nakata, Y. and Okada, T. (1999) Time-resolved microscopic imaging of the laser-induced forward transfer process. *Appl. Phys. A*, **69** (Suppl.), S275–S278.

125. Fitz-Gerald, J.M., Piqué, A., Chrisey, D.B., Rack, P.D., Zelenznik, M., Auyeung, R.C.Y., and Lakeou, S. (2000) Laser direct writing of phosphor screens for high-definition displays. *Appl. Phys. Lett.*, **76**(11), 1386–1388.

126. Lee, J.H., Yoo, C.D., and Kim, Y.-S. (2007) A laser-induced thermal spray printing process for phosphor layer deposition of PDP. *J. Micromech. Microelectron.*, **17**, 258–264.

127. Barron, J.A., Wu, P., Ladouceur, H.D., and Ringeisen, B.R. (2004) Biological laser printing: A novel technique for

creating heterogeneous 3-dimensional cell patterns. *Biomed. Microdevices*, **6**(2), 139–147.

128. Barron, J.A., Krizman, D.B., and Ringeisen, B.R. (2005) Laser printing of single cells: statistical analysis, cell Viability, and stress. *Ann. Biomed. Eng.*, **33**(2), 121–130.

129. Ringeisen, B.R., Othon, C.M., Barron, J.A., Young, D., and Spargo, B.J. (2006) Jet-based methods to print living cells. *Biotechnol. J.*, **1**, 930–948.

130. Fernandez-Pradas, J.M., Colina, M., Serra, P., Dominguez, J., and Morenza, J.L. (2004) Laser-induced forward transfer of biomolecules. *Thin Solid Films*, **453–454**, 27–30.

131. Serra, P., Fernandez-Pradas, J.M., Berthet, F.X., Colina, M., Elvira, J., and Morenza, J.L. (2004) Laser direct writing of biomolecule microarrays. *Appl. Phys. A*, **79**, 949–952.

132. Serra, P., Colina, M., Fernandez-Pradas, J.M., Sevilla, L., and Morenza, J.L. (2004) Preparation of functional DNA microarrays through laser-induced forward transfer. *Appl. Phys. Lett.*, **85**(9), 1639–1641.

133. Colina, M., Serra, P., Fernandez-Pradas, J.M., Sevilla, L., and Morenza, J.L. (2005) DNA deposition through laser induced forward transfer. *Biosens. Bioelectron.*, **20**, 1638–1642.

134. Serra, P., Fernandez-Pradas, J.M., Colina, M., Duocastella, M., Dominguez, J., and Morenza, J.L. (2006) Laser-induced forward transfer: a direct- writing technique for biosensors preparation. *J. Laser Micro/Nanoeng.*, **1**(3), 236–242.

135. Colina, M., Duocastella, M., Fernandez-Pradas, J.M., Serra, P., and Morenza, J.L. (2006) Laser-induced forward transfer of liquids: study of the droplet ejection process. *J. Appl. Phys.*, **99**, 084909-1–084909-7.

136. Duocastella, M., Colina, M., Fernandez-Pradas, J.M., Serra, P., and Morenza, J.L. (2007) Study of the laser-induced forward transfer of liquids for laser bioprinting. *Appl. Surf. Sci.*, **253**, 7855–7859.

137. Duocastella, M., Fernandez-Pradas, J.M., Serra, P., and Morenza, J.L. (2008) Laser-induced forward transfer of liquids for miniaturized biosensors preparation. *J. Laser Micro/Nanoeng.*, **3**(1), 1–4.

138. Duocastella, M., Fernandez-Pradas, J.M., Serra, P., and Morenza, J.L. (2008) Jet formation in the laser forward transfer of liquids. *Appl. Phys. A*, **93**, 453–456.

139. Duocastella, M., Fernández-Pradas, J.M., Domínguez, J., Serra, P., and Morenza, J.L. (2008) Printing biological solutions through laser-induced forward transfer. *Appl. Phys. A*, **93**, 941.

140. Serra, P., Duocastella, M., Fernández-Pradas, J.M., and Morenza, J.L. (2008) Liquids microprinting through laser-induced forward transfer. *Appl. Surf. Sci.*, **255**, 5342.

141. Duocastella, M., Fernández-Pradas, J.M., Morenza, J.L., and Serra, P. (2009) Time-resolved imaging of the laser forward transfer of liquids. *J. Appl. Phys.*, **106**, 084907.

142. Vodp'yanov, L.K., Kozlov, P.S., Kucherenko, I.V., Maksimoviskii, S.N., and Radutskii, G.A. (2003) Studying the possibility of applying the light-hydraulic effect to digital printing. *Instrum. Exp. Tech.*, **46**(4), 549–553.

143. Hopp, B., Smausz, T., Antal, Z., Kresz, N., Bor, Z., and Chrisey, D. (2004) Absorbing film assisted laser induced forward transfer of fungi (Trichoderma conidia). *J. Appl. Phys.*, **96**(6), 3478–3481.

144. Hopp, B., Smausz, T., Barna, N., Vass, C., Antal, Z., Kredics, L., and Chrisey, D. (2005) Time-resolved study of absorbing film assisted laser induced forward transfer of Trichoderma longibrachiatum conidia. *J. Phys. D: Appl. Phys.*, **38**, 833–837.

145. Hopp, B., Smausz, T., Kresz, N., Barna, N., Bor, Z., Kolozsvari, L., Chrisey, D.B., Szabo, A., and Nogradi, A. (2005) Survival and proliferative ability of various living cell types after laser-induced forward transfer. *Tissue Eng.*, **11**(11/12), 1817–1823.

146. Nogradi, A., Hopp, B., Smausz, T., Kecskemeti, G., Bor, Z., Kolozsvari, L., Szabo, A., Klini, A., and Fotakis, C.

(2008) Directed cell growth on laser-transferred 2D biomaterial matrices. *Open Tissue Eng. Regenerative Med. J.*, **1**, 1–7.

147. Smausz, T., Hopp, B., Kecskemeti, G., and Bor, Z. (2006) Study on metal microparticle content of the material transferred with absorbing film assisted laser induced forward transfer when using silver absorbing layer. *Appl. Surf. Sci.*, **252**, 4738–4742.

148. Dinca, V., Kasotakis, E., Catherine, J., Mourka, A., Mitraki, A., Popescu, A., Dinescu, M., Farsari, M., and Fotakis, C. (2007) Development of peptide-based patterns by laser transfer. *Appl. Surf. Sci.*, **254**, 1160–1163.

149. Dinca, V., Farsari, M., Kafetzopoulos, D., Popscu, A., Dinescu, M., and Fotakis, D. (2008) Patterning parameters for biomolecules microarrays constructed with nanosecond and femtosecond UV lasers. *Thin Solid Films*, **516**, 6504–6511.

150. Dinca, V., Kasotakis, E., Mourka, A., Ranella, A., Farsari, M., Mitraki, A., and Fotakis, C. (2008) Fabrication of amyloid peptide micro-arrays using laser-induced forward transfer and avidin-biotin mediated assembly. *Phys. Stat. Sol. C*, **5**(12), 3576–3579.

151. Boutopoulos, C., Andreakou, P., Kafetzopoulos, D., Chatzandroulis, C., and Zergioti, I. (2008) Direct laser printing of biotin microarrays on low temperature oxide on Si substrates. *Phys. Stat. Sol. A*, **205**(11), 2505–2508.

152. Boutopoulos, C., Tsouti, V., Goustouridis, D., Chatzandroulis, S., and Zergioti, I. (2008) Liquid phase direct laser printing of polymers for chemical sensing applications. *Appl. Phys. Lett.*, **93**, 191109-1–191109-4.

153. Tsouti, V., Goustouridis, D., Chatzandroulis, S., Normand, P., Andreakou, P., Ioannou, M., Kafetzopoulos, D., Boutopoulos, C., Zergioti, I., Tsoukalas, D., Hue, J., and Rousier R. (2008) A capacitive biosensor based on ultrathin Si membranes. Reports of the 2008 IEEE Sensors Conference, IEEE Conference Publications, pp. 223–226, doi: 10.1109/ICSENS.2008.4716421

154. Tsouti, V., Boutopoulos, C., Andreakou, P., Ioannou, M., Zergioti, I., Goustouridis, D., Kafetzopoulos, D., Tsoukalas, D., Normand, P., and Chatzandroulis, S. (2009) Detection of the biotin-streptavidin interaction by exploiting surface stress changes on ultrathin Si membranes. *Microelectron. Eng.*, **86**, 1495–1498.

155. Ovsianikov, A., Gruene, M., Pflaum, M., Koch, L., Maiorana, F., Wilhelmi, M., Haverich, A., and Chichkov, B. (2010) Laser printing of cells into 3D scaffolds. *Biofabrication*, **2**, 014104.

156. Rapp, L., Cibert, C., Alloncle, A.P., and Delaporte, P. (2009) Characterization of organic material micro-structures transferred by laser in nanosecond and picosecond regimes. *Appl. Surf. Sci.*, **255**, 5439–5443.

157. Kröger, M., Hüske, M., Dobbertin, T., Meyer, J., Krautwald, H., Riedl, T., Johannes, H.-H., and Kowalsky, W. (2005) A novel patterning technique for high-resolution RGB-OLED displays: laser induced local transfer (LILT). *Mater. Res. Soc. Symp. Proc.*, **807E**, 77–82.

158. Blanchet, G.B., Loo, Y.L., Rogers, J.A., Gao, F., and Fincher, C.R. (2003) Large area, high resolution, dry printing of conducting polymers for organic electronics. *Appl. Phys. Lett.*, **82**(3), 463.

159. DuPont (2008) Displays Brochure *http://www2.dupont.com/Displays/en_US/assets/downloads/pdf/DisplaysBrochure.pdf* (accessed September 2010).

160. Wolk, M.B., Baetzold, J., Bellmann, E., Hoffend, T.R., Lamansky, S., Li, Y., Roberts, R.R., Savvateev, V., Staral, J.S., and Tolbert, W.A. (2004) Laser thermal patterning of OLED materials. *Proc. SPIE*, **5519**, 12–23.

161. Lamansky, S., Hoffend, T.R., Le, H., Jones, V., Wolk, M.B., and Tolbert, W.A. (2005) Laser induced thermal imaging of vacuum-coated OLED materials. *Proc. SPIE*, **5937**, 593702.

162. Chin, B.D., Suh, M.C., Kim, M.H., Kang, T.M., Yang, N.C., Song, M.W., Lee, S.T., Kwon, H.H., and Chung, H.K. (2003) High efficiency AMOLED

using hybrid of small molecule and polymer materials pattered by laser transfer. *J. Inform. Display*, **4**(3), 1–5.

163. Suh, M.C., Chin, B.D., Kim, M.-H., Kang, T.M., and Lee, S.T. (2003) Enhanced luminance of blue light-emitting polymers by blending with hole-transporting materials. *Adv. Mater.*, **15**(15), 1254–1258.

164. Lee, J.Y. and Lee, S.T. (2004) Laser-induced thermal imaging of polymer light-emitting materials on poly(3,4-ethylenedioxythiophene): silane hole-transport layer. *Adv. Mater.*, **16**(1), 51–54.

165. Dinca, V., Fardel, R., Shaw-Stewart, J., Di Pietrantonio, F., Cannatà, D., Benetti, M., Verona, E., Palla-Papavlu, A., Dinescu, M., and Lippert, T. (2010) Laser-induced forward transfer: an approach to single-step polymer microsensor fabrication. *Sens. Lett.*, **8**, 436–440.

166. Nagel, M., Hany, R., Lippert, T., Molberg, M., Nüesch, F.A., and Rentsch, D. (2007) Aryltriazene photopolymers for UV-laser applications: improved Synthesis and photodecomposition study. *Macromol. Chem. Phys.*, **208**, 277–286.

167. Lippert, T. (2004) Laser applications of polymers in polymers and light. *Adv. Polym. Sci.*, **168**, 51–246, and references therein.

168. Fardel, R., Feurer, P., Lippert, T., Nagel, M., Nüesch, F.A., and Wokaun, A. (1887) Laser ablation of aryltriazene photopolymer films: effects of polymer structure on ablation properties. *Appl. Surf. Sci.*, **254**, 1332–1337.

169. Mito, T., Tsujita, T., Masuhara, H., Hayashi, N., and Suzuki, K. (2001) Hollowing and transfer of polymethyl methacrylate film propelled by laser ablation of triazeno polymer film. *Jpn. J. Appl. Phys.*, **40** (Part 2, 8A), L805–L806.

170. Fardel, R., Nagel, M., Nüesch, F., Lippert, T., and Wokaun, A. (2007) Laser forward transfer using a sacrificial layer: Influence of the material properties. *Appl. Surf. Sci.*, **254**, 1322–1326.

171. Dinca, V., Fardel, R., Di Pietrantonia, F., Cannata, D., Benetti, M., Verona, E., Palla-Papavlu, A., Dinescu, M., and Lippert, T. (2010) Laser-induced forward transfer: An approach to single-step polymer microsensor fabrication. *Sens. Lett.*, **8**, 1–5.

172. Fardel, R., Nagel, M., Lippert, T., Nüesch, F., Wokaun, A., and Luk'yanchuk, B.S. (2008) Influence of thermal diffusion on ablation of thin polymer films. *Appl. Phys. A*, **90**, 661–667.

173. Nagel, M., Fardel, R., Feurer, P., Häberli, M., Nüesch, F.A., Lippert, T., and Wokaun, A. (2008) Aryltriazene photopolymer thin films as sacrificial release layers for laser-assisted forward transfer systems: study of photoablative decomposition and transfer behaviour. *Appl. Phys. A*, **92**, 781–789.

174. Shaw Stewart, J., Fardel, R., Nagel, M., Delaporte, P., Rapp, L., Cibert, C., Alloncle, A.-P., Nüesch, F., Lippert, T., and Wokaun, A. (2010) The effect of laser pulse length upon laser-induced forward transfer using a trazene polymer as dynamic release layer. *J. Optoelectron. Adv. Mater.*, **12**(3), 605–609.

175. Doraiswamy, A., Narayan, R.J., Lippert, T., Urech, L., Wokaun, A., Nagel, M., Hopp, B., Dinescu, M., Modi, R., Auyeung, R.C.Y., and Chrisey, D.B. (2006) Excimer laser forward transfer of mammalian cells using a novel triazene absorbing layer. *Appl. Surf. Sci.*, **252**, 4743–4747.

176. Schiele, N.R., Koppes, R.A., Corr, D.T., Ellison, K.S., Thompson, D.M., Ligon, L.A., Lippert, T.K.M., and Chrisey, D.B. (2009) Laser direct writing of combinatorial libraries of idealized cellular constructs: Biomedical applications. *Appl. Surf. Sci.*, **255**, 5444–5447.

177. Xu, J., Liu, J., Cui, D., Gerhold, M., Wang, A.Y., Nagel, M., and Lippert, T.K. (2007) Laser-assisted forward transfer of multi-spectral nanocrystal quantum dot emitters. *Nanotechnology*, **18**, 025403 (6pp).

178. Fardel, R., Nagel, M., Nüesch, F., Lippert, T., and Wokaun, A. (2007) Fabrication of organic light-emitting

diode pixels by laser-assisted forward transfer. *Appl. Phys. Lett.*, **91**, 061103.

179. Fardel, R., Nagel, M., Nüesch, F., Lippert, T., and Wokaun, A. (2009) Shadowgraphy investigation of laser-induced forward transfer: front side and back side ablation of the triazene polymer sacrificial layer. *Appl. Surf. Sci.*, **255**, 5430–5434.

180. Fardel, R., Nagel, M., Nüesch, F., Lippert, T., and Wokaun, A. (2009) Energy balance in a laser-induced forward transfer process studied by shadowgraphy. *J. Phys. Chem. C*, **113**, 11628–11633.

181. Kaur, K., Fardel, R., May-Smith, T.C., Nagel, M., Banks, D.P., Grivas, C., Lippert, T., and Eason, R.W. (2009) Shadowgraphic studies of triazene assisted laser-induced forward transfer of ceramic thin films. *J. Appl. Phys.*, **105**(11), 113119.

182. Fardel, R., Nagel, M., Nüesch, F., Lippert, T., and Wokaun, A. (2010) Laser-induced forward transfer of organic LED building blocks studied by time-resolved shadowgraphy. *J. Phys. Chem. C*, **114**, 5617–5636.

183. Bonse, J., Solis, J., Urech, L., Lippert, T., and Wokaun, A. (2007) Femtosecond and nanosecond laser damage therhods of doped and undoped trazenepolymer thin films. *Appl. Surf. Sci.*, **253**, 7787–7791.

184. Banks, D.P., Kaur, K., Gazia, R., Fardel, R., Nagel, M., Lippert, T., and Eason, R.W. (2008) Triazene photopolymer dynamic release layer-assisted femtosecond laser-induced forward transfer with an active carrier substrate. *Europhys. Lett.*, **83**, 38003.

185. Banks, D.P., Kaur, K.S., and Eason, R.W. (2009) Influence of optical standing waves on the femtosecond laser-induced forward transfer of transparent thin films. *Appl. Opt.*, **48**(11), 2058–2066.

186. Banks, D.P., Grivas, C., Mills, J.D., Eason, R.W., and Zergioti, I. (2006) Nano-droplets deposited in microarrays by femtosecond Ti:sapphire laser-induced forward transfer. *Appl. Phys. Lett.*, **89**, 193107.

187. Banks, D.P., Grivas, C., Zergioti, I., and Eason, R.W. (2008) Ballistic laser-assisted solid transfer (BLAST) of intact material from a thin film precursor. *Opt. Express*, **16**(5), 3249–3254.

188. Banks, D.P., Kaur, K.S., and Eason, R.W. (2009) Etching and forward transfer of fused silica in solid-phase by femtosecond laser-induced solid etching (LISE). *Appl. Surf. Sci.*, **255**(20), 8343–8351.

189. Vogel, A., Lorenz, K., Herneffer, V., Hüttmann, G., Smolinski, D., and Gebert, A. (2007) Mechanisms of laser-induced dissection and transport of histologic specimens. *Biophys. J.*, **93**, 4481–4500.

190. Horneffer, V., Linz, N., and Vogel, A. (2007) Principles of laser-induced separation and transport of living cells. *J. Biomed. Opt.*, **12**(5), 054016-1–054016-13.

191. Kattamis, N.T., Purnick, P.E., Weiss, R., and Arnold, C.B. (2007) Thick film laser induced forward transfer for deposition of thermally and mechanically sensitive materials. *Appl. Phys. Lett.*, **91**, 171120.

192. Kononenko, T.V., Alloncle, P., Konov, V.I., and Sentis, M. (2009) Laser transfer of diamond nanopowder induced by metal film blistering. *Appl. Phys. A*, **94**, 531–536.

193. Holmes, A.S. and Saidam, S.M. (1998) Sacrificial layer process with laser-driven release for batch assembly operations. *J. Micromech. Syst.*, **7**(4), 416–422.

194. Piqué, A., Charipar, N.A., Auyeung, R.C.Y., Kim, H., and Matthews, S.A. (2007) Assembly and Integration of thin bare die using laser direct write. *Proc. SPIE*, **6458**, 645802.

195. Mathews, S.A., Auyeung, R.C.Y., and Piqué, A. (2007) Use of laser direct-write in microelectronics assembly. *J. Laser Micro/Nanoeng.*, **2**(1), 103–107.